β-catenin-promoted cholesterol metabolism protects against cellular senescence in naked mole-rat cells

A Doctoral Thesis

by

Woei-Yaw Chee

Department of Oncogene Research
Research Institute for Microbial Diseases
Osaka University

February 2021

INDEX

LIST OF FIGURES

β-catenin-promoted cholesterol metabolism protects against cellular senescence in naked mole-rat cells

The naked mole-rat (NMR; *Heterocephalus glaber)* exhibits cancer resistance and an exceptionally long lifespan of approximately 30 years. The longevity of the NMR is widely debated, as it poses challenges to theories associated with aging, cancer, and redox homeostasis. In the present study, I report unique mechanisms of cholesterol metabolism in NMR cells that could be responsible for their anti-senescent properties. I found that NMR fibroblasts abundantly express β-catenin, and that increased β-catenin activity is linked to increased accumulation of cholesterol-enriched lipid droplets. Either β-catenin knockdown or inhibition of cholesterol synthesis abolished lipid droplet formation and enhanced induction of senescence-like phenotypes. Analysis of β-catenin-regulated genes revealed that β-catenin upregulated apolipoprotein F and the LXR/RXR pathway, which are involved in cholesterol transport and biogenesis. Specifically, genetic ablation of apolipoprotein F suppressed lipid droplet accumulation and promoted cellular senescence, indicating that apolipoprotein F is a critical mediator of the β-catenin signaling in NMR cells. Thus, I suggest that increased β-catenin activity evolved in NMRs to offset senescence via the accumulation of cholesterol-enriched lipid droplets. Hence, the anti-senescence effects of the β-catenin signaling reveal new strategies for longevity in NMRs.

CHAPTER I

INTRODUCTION

1.1 Background

The research outlined in this dissertation is to understand the significance of the β-catenin pathway in *Heterocephalus glaber*, also known as the Naked Mole Rat (NMR), which serves as a primary pathway in preventing senescence. Firstly, this research investigates how the inhibition or modified regulation of the Wnt/β-catenin signalling pathway would cause changes in cell proliferation rate and morphological changes. The research was then further explored to determine how the altered mechanism of β-catenin signalling would affect the regulation of cholesterol metabolism involved in anti-senescence in naked mole-rat.

Hence, with the information presented above, it was tremendously exciting to explore the complexities caused by the changes of β-catenin regulation in NMR cells and to investigate whether the altered β-catenin concentration would disrupt and interfere with the anti-senescent mechanism driven by the abundance of cholesteryl esters in NMR. Before outlining the rationale of this research, it is necessary to establish some information relevant to NMR and core proteins involved in the Wnt/β-catenin signaling pathway in the subsequent sections.

1.2 Naked Mole Rat

Naked mole-rats (NMRs; *Heterocephalus glaber*) are renowned for their exceptional longevity, and remarkable resistance to cancer [1,2], with only two cases of cancer, are reported in zoo-housed NMR after multiyear observation of large colonies [3]. Besides that, NMRs are strictly subterranean, eusocial mammals that live in a chronically low-oxygen environment [4], justifying its incredible resistance to hypoxia [5]. Astonishingly, this species can survive in condition deprived of oxygen (anoxia) for 18 minutes without apparent injury [6]. Despite accumulating considerable levels of oxidative damage and protein carbonylation than mice, NMR appears to be resilient to oxidative stress and mitochondrial injury and strikingly accompanied with a slower aging rate, contributing to their enhanced longevity [7-9]. Besides, NMRs display negligible senescence accompanied by high fecundity, and most importantly, it remains healthy and shows resistance to age-related disease until death [10]. Therefore, the naked mole-rat has been increasingly utilized as an animal model in aging and cancer research because of the characteristics mentioned above. Several cancer-resistance models have been described in this species: For instance, in tissue culture, NMR fibroblast displayed extreme sensitivity of their cells to contact inhibition, which serves as an efficient anti-cancer mechanism regulated by the INK4 locus [11]. Another study conducted by Tian et al 2013 showed that hyaluronan, a high molecular mass weight polysaccharide of the extracellular matrix, is the signal that triggers the early contact inhibition. Even the addition of a combination of oncoproteins that could result in tumour formation in mouse cells could not malignantly transform the naked mole-rat cells [12], corroborating the fact that NMR is resistant to both spontaneous cancer and experimentally induced tumorigenesis [13]. However, knockdown of hyaluronan synthase 2 (HAS2) gene or overexpression of hyaluronoglucosaminidase 2 (HYAL2) gene resulted in the removal of high molecular mass hyaluronan, abrogating the activity of ECI and rendered the NMR cells susceptible to malignant transformation.

1.3 Wnt/β-catenin pathway

he Wnt signalling pathway is an ancient system that has been highly conserved during evolution. Upon Wnt pathway activation, β-catenin accumulates in the cytoplasm and nucleus, where it engages DNA-bound TCF transcription factors, leading to the embryonic development of all animal species in the regeneration of tissues in the adult organism and in many other cellular responses (Figure A). Mutation or deregulated expression of the Wnt pathway components an induce disease, most notably cancer [14]. In the following sections, β-catenin, Axin1, APC and GSK3β will be reviewed.

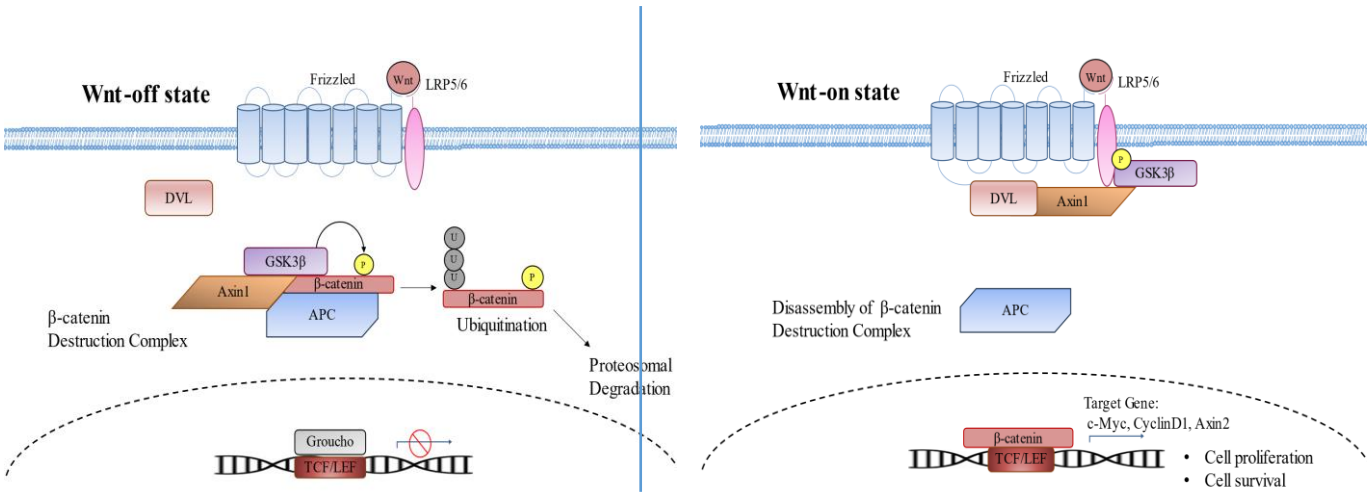

Figure A. The catenin-dependent or canonical Wnt signalling pathway [15].

1.3.1 β-catenin

The central effector in the canonical Wnt pathway is the cytoplasmic protein β-catenin. The destruction complex regulates its stability consist of the tumour suppressor protein Axin1, APC, and two constitutively active serine-threonine kinases CK1α and GSK3β. In this complex, Axin1 acts as the scaffold, interacting with β-catenin, APC, GSK3β, and CK1α. The APC protein contains three Axin-binding motifs that are interspersed between a series of 15 and 20 amino acid repeats that bind β-catenin. In the absence of Wnt ligands, β-catenin is phosphorylated sequentially by CK1α and GSK3β at a series of regularly spaced N-terminal Ser/Thr moieties. At first, β-catenin

is phosphorylated by CSK1α at Ser45, followed by GSK3β phosphorylation at Thr41, Ser37, and Ser33 residues [16]. Then, the phosphorylated "degron" motif is targeted by E3 ubiquitin ligase (β-TrCP) for ubiquitination and subsequent proteasomal degradation [17,18]. Moreover, in the Wnt off state, TCF interacts with Groucho proteins to mediate transcriptional repression [19,20]. On the contrary, when Fr/LRP is engaged with Wnt ligands, the receptors relocalize the destruction complex to the cell membrane and interferes with the latter activity, causing rapid elevation of free β-catenin. Simultaneously, GSK3β is directly inhibited by the phosphorylated LRP receptor, promoting β-catenin stabilization [21]. The accumulation of free β-catenin then translocates into the nucleus, where it engages DNA-bound TCF transcription factors to initiate Wnt target genes such as Cyclin D1 [22], c-Myc [23], and EPB [24].

Active Wnt signalling may involve an increase in overall β-catenin levels without any detectable nuclear accumulation. It has been suggested that fold-change rather than absolute β-catenin level are critical, implying that the low level of β-catenin is sufficient for target gene activation [25]. As previously described, while most Wnt target genes are cell type and developmental stage-specific, the Axin2 gene represents a generic transcriptional target gene and is often used as an indicator of canonical Wnt pathway activity [26]. Besides being a transcriptional activator, β-catenin plays a structural role in mediating the interaction between the cell adhesion complex and the actin cytoskeleton in epithelia. While the half-life of the signaling pool of β-catenin is in the order of minutes, the adherent junction pool is highly stable. The adhesive and signalling pretties of β-catenin are most likely independent.

1.3.2 Axin

Vertebrates have two Axin isoforms: Axin1 is constitutively expressed, while Axin2 (Conductin) is subjected to Wnt signalling[27,28]. Axin1, an essential component of the canonical Wnt pathway, plays dual roles in modulating Wnt signalling. The predominant role of Axin1 is to scaffold a multiprotein destruction complex, which drives the phosphorylation and subsequent proteolysis of the transcriptional regulator β-catenin [29-31], Furthermore, owing to its very low abundance, it also represents a rate-limiting factor for complex activity [32]. Secondly, Axin1 interacts with LRP5/6 and facilitates the recruitment of GSK3β to the plasma membrane to promote LRP5/6

phosphorylation and Wnt signalling [33]. To date, there are multiple mechanisms revealed in the regulation of Axin1 activity, including post-translational modulation [34], homo/heteropolymerization [35], and autoinhibition [36]. These mechanisms might work cooperatively to mediate the function of Axin1, thereby playing an essential role in controlling the canonical Wnt signalling. Strikingly, the mutational spectrum in Axin1 shows a higher prevalence of missense mutation rather than deletion and truncation. The missense mutated Axin1 forms non-amyloid aggregates with disordered "tails," rewiring the Axin1 interactome and derail Wnt signalling [37]. Furthermore, Axin1 mutation is frequently accompanied by a gain in copy number and mRNA overexpression, further promoting tumour growth *in vivo* through a gain-of-function mechanism.

On the other hand, Axin2 can inhibit β-catenin abundance and function, therefore implying that Axin2 is part of the negative feedback mechanism in regulating in Wnt pathway[38]. Although Axin1 and Axin2 have been thought to have comparable functions the observation that Wnt pathway activation elevates Axin2 instead of Axin1 expression suggest that there may be potentially significant functional differences between two proteins [38].

1.3.3 Adenomatous polyposis coli (APC)

Mutational inactivation of APC tumour suppressor genes is renowned for a common precursor to initiate the various forms of colorectal carcinomas via the development of adenomatous polyp [39]. Most mutation in the APC genes tend to cluster at Mutation Cluster Region, where the introduction of stop codons leads to expression of truncated APC lacking carboxy terminus [40]. Additionally, several studies have identified a highly conserved regulatory domain in APC, the β-catenin inhibitory domain (CID), located between the second and the third 20 amino acid repeats [41,42]. The CID is believed to be essential for downregulating β-catenin levels and Wnt transcriptional activity. In agreement, the CID is located right at the mutation cluster region, the site of common truncation of APC in cancer. The CID has been proposed to promote β-catenin ubiquitination by stabilizing the association with APC as well as to repress β-catenin/TCF transcription in the nucleus [43].

These extensive studies are to underscore that the imperative function of the APC protein is the regulation of cytoplasmic β-catenin levels by improving β-catenin binding to the APC-mediated destruction complex, followed by GSK3β-dependent phosphorylation which eventually targeting the β-catenin for proteolysis [44-46]. In addition to its roles in Wnt pathway, APC is also a nucleocytoplasmic shuttling protein found in several subcellular compartments of mammalian and *Drosophila* cells including the cytoplasm, nucleus and adhesive cadherin/catenin function [47]. Recently, APC has been reported to promote the export of β-catenin from the nucleus, reducing the amount of nuclear β-catenin/TCF complex [48-50].

Hence, dysfunction in APC contributes to early event of tumorigenesis by causing an aberrant accumulation of β-catenin, which then binds to T-cell factor 4 (TCF4), leading to enhanced transcriptional activation of Wnt-target genes. In addition, the Wnt pathway is commonly involved in neoplastic transformation of mammalian cells [51,52], as highlighted by the findings in which mutations in the β-catenin gene that hinders APC-mediated phosphorylation and proteolytic degradation [53,54], are often found in colon and other tumours.

13.4 Glycogen Synthase Kinase 3β

GSK3β is a multifunctional serine/threonine kinase contributing to a vast majority of processes such as cell polarity, transcription, endocytosis and cytoskeletal regulation. Numerous GSK3β substrates have been identified and categorized into primed substrates and unprimed substrates [55]. Primed substrates including β-catenin, require the priming phosphorylation by another kinase (CK1α in in canonical Wnt pathway) at serine/threonine residue located near the GSK3β phosphorylation site [56,57]. On the other hand, unprimed substrates, such as Axin-1, low-density lipoprotein receptor-related 6 (LRP6), and also GSK3β substrates do not require the priming phosphorylation [30,58,59]. Inactivation of GSK3β is regulated through phosphorylation at specific residues. For instance, phosphorylation at Ser9 of GSK3β is modulated by Akt and other kinases is the general mechanism of GSK3β inactivation [60,61]. Besides that, phosphorylation at Ser389 by p38 MAPK serve as an alternative pathway for GSK3β inactivation [62].

1.4 Significant statement

The naked mole-rat (NMR; *Heterocephalus glaber)* is remarkably cancer-resistant, even with an exceptionally long lifespan of approximately 30 years. However, the molecular mechanisms underlying these unique features remain elusive. I performed comparative analyses of oncogenic signals between NMR cells and mouse cells, and found that in NMR cells, β-catenin signaling, which generally promotes cell proliferation in other mammals, was increased. Furthermore, constitutively active β-catenin signaling protected NMR cells from senescence by promoting cholesterol metabolism and transport. These findings reveal a new paradox that can be exploited for the development of anti-aging therapeutics.

1.5 Aim and Objectives of this work

1.5.1 aim

This research aims to investigate the hypothesis that NMR β-catenin is governing the regulation of cholesterol metabolism via a unique pathway, affecting the onsets and activation of the senescence process.

1.5.2 Objectives

This research is designed to achieve the following objectives:

- To determine whether the **reduction of β-catenin** using shRNA or siRNA technique could c**ontribute to cellular senescence in NSF**.
- To identify the **functional target genes** of β-catenin using RNA-seq.
- To investigate the **correlation between β-catenin and formation of lipid droplets abundance**

CHAPTER II

MATERIALS AND METHODS

2.1 Materials (Antibodies and Chemicals)

Antibodies and chemicals

Alexa Fluor 488-phalloidin, Alexa Fluor 594-goat anti-rabbit IgG, HRP-conjugated goat anti-rabbit IgG, and HRP-conjugated goat anti-mouse IgG were purchased from Thermo Fisher Scientific (Waltham, MA, USA). Anti-β-catenin (D10A8), anti-phospho-β-catenin (pSer41), anti-Axin1 (C76H11), anti-GSK-3β, anti-phospho-GSK-3β (pSer9), anti-cyclin D1, and anti-p21 antibodies were from Cell Signaling Technology (Beverly, MA, USA). The anti-8-OHdG (15A3) antibody was purchased from Santa Cruz Biotechnology (Dallas, TX, USA) and anti-β-tubulin was purchased from Sigma Aldrich (St Louis, Mo, USA). The anti-ApoF (ab231585) antibody was purchased from Abcam (Cambridge, MA, USA). The protease inhibitor cocktail was purchased from Nacarai Tesque (Kyoto, Japan). ORO and triethyl-phosphate [$(C_2H_5O)_3PO$] were purchased from WAKO (Osaka, Japan). Lovastatin was purchased from Merk (Darmstadt, Germany).

2.2 Methods

2.2.1 Cell lines and Tissue Culture

Primary adult NMR fibroblasts were received from Department of Aging and Longevity Research, Kumamoto University. MSFs were prepared from adult mouse skin, and NIH

3T3 cells were obtained from American Type Culture Collection. To investigate whether temperature, oxygen concentration, or serum concentration affect β-catenin expression or lipid droplets abundance within the cells, both NMR cell lines and mouse cell lines were cultured in Dulbecco's modified Eagle's medium (DMEM) supplemented with 10% FBS or 15% FBS at hypoxic (5.0% CO_2, 3.0% O_2) or normoxic (5.0% CO_2, 16.5% O_2) conditions at 32°C or 37°C. Upon reaching 70-80% confluences, the cells were harvested for lysate collection. To maintain the optimal culture condition for NMR cell lines, both primary NMR fibroblasts and mouse fibroblasts between passage numbers 1–13 were grown in Dulbecco's modified Eagle's medium (DMEM) supplemented with 15% (v/v) fetal bovine serum (FBS) at 32°C in a 5.0% CO_2 and 3.0% O_2 atmosphere, as described previously [63].

2.2.2 Inactivation of Wnt signaling

The Wnt production inhibitor, IWP-2 (Selleck Chemicals), was used to inactivate Wnt signaling in NMR fibroblasts. NMR fibroblasts were plated at 500,000 cells per well in 6-well plates. After 48-hours, cells were treated with vehicle (0.1% DMSO) or IWP-2 in a dose-dependent manner up to 100 μM, following by lysate collection for immunoblotting after 48-hours. For the inhibition of the interaction between β-catenin and TCF-4, small-molecule compound PNU-74654 (Selleck Chemicals) was used at the concentration of 50μM, 100μM, and 200μM in NMR and mouse skin fibroblasts 48-hours after seeding.

2.2.3 Plasmid constructs and shRNA constructs

To generate β-catenin shRNA, the sequences were designed to target the central and UTR regions, and the silent constructs were subcloned into the pLKO1 lentiviral vector. ApoF and β-catenin cDNA was generated by PCR using NMR and mouse cDNA as a template respectively. The ApoF and β-catenin constructs was then subcloned into the CSII-CMV-MCS-IRES-Bsd lentiviral (RIKEN) and PCX4 retroviral vector respectively. All generated constructs were confirmed by sequencing. The pLKO1 Non-Target shRNA control plasmid was purchased from Sigma Aldrich. The

oligonucleotide sequences used to generate shRNA vectors in this study were listed in Supplemental Table S3.

2.2.3 Retroviral and lentiviral infection

For knockdown experiment, lentiviral shRNA targeting NMR β-catenin and ApoF; or an empty vector construct was packaged in HEK293T cells with pLKO1 vector with packaging genes Vsv-G, Gag-pol, and Rev from MISSION Lentiviral packaging mix (Sigma-Aldrich) using Lipofectamine 3000 as a transfection reagent. The 293T culture medium containing the lentiviral particles was collected, filtered with 0.2-μm syringe filter (Whatman), and supplemented with 4μg/mL Polybrene (Nacalai Tesque). For transduction, cells cultured in a 6cm plate were incubated with 2 mL filtered virus-containing medium and growth medium in 1:1 ratio overnight. This point was designated day 0. The viral medium was then replaced with fresh growth medium on day 1 post-transduction. On day 3 post-transduction, the transduced cells were then selected by growing with 10μg/mL puromycin. For overexpression of ApoF in NMR cells, lentiviral packaging vector (pcAG-HIVgp), Rev-expressing vector (pCMV-VSV-G-RSV-Rev), and CSII-CMV-MCS-IRES-Bsd lentiviral vector containing NMR ApoF genetic construct were transfected into PLT cells using FuGene (Promega, Madison, WI, USA, and the culture supernatant was used as the source of the virus, followed by transduction into NSFs as described previously in this context. In dual lentiviral transfection, the second transduction was conducted on day 7 post-transduction. For β-catenin overexpression, retroviral vector PCX4 was used for transduction in mouse cell lines. The production and infection of retroviral vectors were performed as described previously [64].

2.2.4 RNA-sequencing

Prior to RNA-sequencing, the puromycin-selected cells were harvested on day 7 post-transduction and were replated onto 6-cm dish with cell count of $1x10^6$. The medium containing puromycin was changed every other day until it reached 80% confluences. NSF shControl (Empty vector) and shβ-catenin #1 were used with no replication in RNA-seq. Total RNA was extracted using Sepasol-G (Nacalai Tesque) according to the

manufacturer's protocol. Library preparation was performed using a TruSeq stranded mRNA sample prep kit (Illumina, San Diego, CA) according to the manufacturer's instructions. Sequencing was performed on an Illumina HiSeq 2500 platform in a 75 bp pair-end mode. Illumina Casava1.8.2 software used for base-calling. Sequenced reads were mapped to the naked mole-rat reference genome sequences (GCA_000247695.1) using TopHat v2.0.13 in combination with Bowtie2 ver. 2.2.3 and SAMtools ver. 0.1.19. The fragments per kilobase of exon per million mapped fragments (FPKMs) were calculated using Cufflinks version 2.2.1. For further analysis, the 216 genes with more than 4-fold change were detected using Ingenuity Pathway Analysis (IPA) [65].

2.2.5 Immunoblotting

Cells were lysed in RIPA buffer (20 mM Tris-HCl pH 7.4, 150 mM NaCl, 0.5 mM EDTA, 1% NP40, 1 mM PMSF, 1mM sodium orthovanadate, 50 mM NaF, and sodium deoxycholate) in combination with protease inhibitor (Invitrogen), and protein concentration was determined using a Bradford protein assay (BioRad). Ten micrograms of denatured lysates were subjected to 10% SDS-PAGE, and blotted using standard procedures. For protein detection, blots were incubated with primary antibodies overnight and with secondary antibodies (rabbit-HRP; G.E. Healthcare) for 30 min. Chemiluminescence was used to visualize the protein bands (G.E. healthcare)

2.2.6 Oil red O staining

Cells were seeded onto tissue cultured chamber slides (25–50% confluency) and allowed to grow for 48-hours before staining. Cells were washed briefly with PBS, followed by cell fixation using 3.7% formaldehyde for 1-hour. Excess formaldehyde was removed by three brief rinses in deionized water. Prior to staining, 35 mg ORO was dissolved in 10 mL of 2-propanol or 6 mL of triethyl-phosphate (TEP) and used as a stock solution [66]. A working solution of ORO containing 6 mL ORO stock solution and 4 mL deionized water was prepared, followed by filtering (0.2 μm). Subsequently, the slides were immersed in the working solution of ORO for 5 min.

2.2.7 Immunofluorescence

Cells were seeded onto tissue culture chamber slides (25–50% confluency) and allowed to grow for 24–36 hours before fixation (manipulation). For experiments involving tracking of cholesterol ester and visualization of oxidative stress in cells, media containing BODIPY CholEster C_{12} (Thermo Fisher Scientific) and CellRox Green (Thermo Fisher Scientific) was incubated for 2-hours prior to fixation. Cells were rinsed in PBS (10 mM phosphate, pH 7.5/100 mM NaCl) and then fixed with 4% paraformaldehyde in PBS for 10 min at room temperature. Following PBS rinsing, cells were permeabilized with 0.1% Triton X-100 in PBS (TPBS) for 10 min at room temperature. Cells were then incubated with 2% BSA for 1-hour at room temperature. Cells were rinsed with TPBS and then incubated at 4°C overnight with primary antibody diluted in antibody buffer (Blocking One). On the following day, cells were rinsed three times with TPBS before incubation with secondary antibody conjugated to fluorescein (AlexaFluor) for 30 min to 1-hour at room temperature. Cells were then rinsed three times with TPBS and mounted with ProLong Gold (Molecular Probes) for immunofluorescence microscopy. For combined immunofluorescence and ORO staining, after three exchanges of PBS following the application of appropriate conjugated fluorescein, glass slides were immersed in the working solution of ORO for 5 minutes. Slides were rinsed three times with deionized water, followed by mounting with ProLong Gold.

2.2.8 TEM

Cells were cultured on a polystyrene coverslip, Cell Desk (Sumitomo Bakelite Co., Ltd., Japan), fixed with 2% formaldehyde and 2.5% glutaraldehyde in 0.1 M sodium-phosphate buffer (pH 7.4) and washed for 5 min three times in the same buffer. Cells were post-fixed for 1-hour with 1% osmium tetroxide and 1% potassium ferrocyanide in 0.1 M sodium-phosphate buffer (pH 7.4), dehydrated in graded series of ethanol, and embedded in Epon812 (TAAB Co. Ltd., U.K.). 80 nm ultra-thin sections were stained with saturated uranyl acetate and lead citrate solution. Electron micrographs were obtained with a JEM-1400plus transmission electron microscope (JEOL, Japan).

2.2.9 TOPFLASH reporter assay

Cells were seeded into 24-well plates as triplicates at a density of 5×10^4 cells/well in a total volume of 500 μL complete growth medium. On the subsequent day, the cell lines were transfected with reporter vectors (ratio of FOPFLASH/TOPFLASH-Firefly luciferase: pRL-TK-Renilla luciferase as 10:1) using Lipofectamine 3000 (Invitrogen), in which the pRL-TK reporter vector was used as an internal control. Twenty-four hours after transfection, luciferase activities were measured using a PicaGene Dual Sea Pansy Luminescence Kit (Wako).

2.2.10 Cell proliferation assay

Cells were plated on a 96-well dish at a density of 500 cells/well in a total volume of 100 μL complete growth medium. After the cells were fully attached to the surface of the dish, 10 μL Cell Counting Kit WST-8 (Doujin Chemistry Laboratories) was added to each well, followed by 1-hour incubation at 32°C. Cell densities were then determined using a microplate reader at the absorbance of 450 nm. In the subsequent days, cell densities were measured at different time points, and growth rates were plotted from 7 to 20 days in culture.

2.2.11 SA-β-Gal assay

Cells were seeded at 2×10^4 cells/well in a 12-well plate 48-hours prior to staining. Cells were washed briefly with cold PBS before being fixed in 1 mL 0.5% glutaraldehyde, followed by incubation at 4°C for 5 min. Cells were then stained with 2 mL freshly prepared 5-bromo-4-chloro-3-indoyl-□-D-galactopyranoside (X-Gal) staining solution, followed by incubation at 37°C for 5-hour. The staining procedure was terminated by washing three times with cold PBS for 5 min. Colour images of X-Gal-stained cells were captured with Bright-Field settings, mounted on an inverted light microscope, using a 10× objective. The stained cells were counted and analyzed manually. Image J analysis was utilized to confirm consistency. Chlorophenolred □-D-galactopyranoside (CPRG) was also used for the quantitative analysis of SA-β-Gal activity.

2.2.12 RT-PCR

RNA was extracted from cells with Sepasol-RNA I Super G (Nacalai Tesque), followed by reverse transcription to obtain the cDNA using the ReverTra Ace qPCR RT Master Mix (TOYOBO). PCR was then performed, and the intensity of DNA bands stained by SYBR gold was quantified using ImageJ analysis. The nucleotide sequences of primers used are listed in Supplemental Table S4.

2.2.13 Cholesterol assay

Cells were seeded at 1×10^5 cells/well in a 6-well plate 48-hours prior to cholesterol extraction. Cells were washed briefly with cold PBS twice, then 1 mL of hexane: isopropanol (3:2) was added to the wells for lipid extraction, followed by incubation at room temperature for 30 minutes. The mixture containing lipids was recovered in Eppendorf tube and was air-dried using Iwaki Halogen Vacuum Concentrator (IVC-500) for 20 minutes at room temperature. The pellet was then resuspended, and cholesterol contents were determined using Amplex Red ™ Cholesterol Assay Kit (Invitrogen). For reloading cholesterol, cholesterol-methyl-β-cyclodextrin (C4951, Sigma) was added to the culture media at the final concentration of 10μg/mL for 24-hours incubation [67,68]. Incorporation of cholesterol into cells was estimated by adding CholEsteryl BODIPY FL C_{12} (Thermo Fisher Scientific) to culture media at the concentration of 5μM for 2-hours incubation before fixation for immunofluorescence.

2.2.14 Alamar Blue Assay

Cultures were set up in a complete media (DMEM supplemented with 15% (v/v) fetal bovine serum (FBS), penicillin/streptomycin, 2 mM L-glutamine (Nakalai Tesque) and 0.1 mM non-essential amino acids (NEAA, Nakalai Tesque) at 1×10^4 cells/well in a 24-well plate. Cultures were incubated for 48-hours, followed by replacement of fresh medium with addition of AlamarBlue Reagent (Thermo Fisher Scientific) at 9:1 ratio. After 12-hours of incubation with Alamar Blue, the medium with fluorescence was collected and was calorimetrically measured at an absorbance of 570nm (Oxidized form of AlamarBlue Reagent) and 600nm (Reduced form). The percentage reduction of the cell or cell viability was calculated using the formula stated in the existing protocol.

2.2.15 Soft-agar colony-formation assay

Soft-agar colony-formation assay was performed as described [69]. Single-cell suspensions of 1×10^4 cells were plated in 12-well culture dishes in 1.5 ml of DMEM containing 15% FBS and 0.36% agar on a layer of 2.5 ml of the same medium containing 0.7% agar. Colonies were stained with 3-(4,5-dimethylthiazol-2-yl)- 2,5-diphenyltetrazolium bromide (MTT) 14 days after plating, and micrographs were used to count the numbers of colonies.

2.2.16 Statistics and reproducibility

All results were depicted as mean ± s.e.m of at least three biological replicated, as indicated in figure legends using GraphPad Prism 7. For data analyses, unpaired two-tailed *t*-tests or ordinary one-way or two-way ANOVA were used to determine the *P*-values. **P*-value <0.05, ***P*-value <0.01, ****P*-value <0.001.

CHAPTER III

RESULTS

3.1 Altered Wnt/β-catenin pathway in NMR cells

I first compared expression levels of various components in oncogenic signaling pathways in NMR skin/lung fibroblasts (NSFs/NLFs), mouse skin fibroblasts (MSFs), and NIH 3T3 cells. I found that β-catenin, a critical transcriptional regulator of the Wnt/β-catenin pathway, was markedly upregulated in NMR cells compared to mouse cells, yet the inactive phosphorylated form of β-catenin was undetectable (**Fig. 1a**). I also found the expression of Axin1, a negative regulator of Wnt signaling, was markedly downregulated in NMR cells (**Fig. 1a**). Immunofluorescence analysis revealed that β-catenin was widely distributed in both the cytoplasm and nucleus of NSFs (**Fig. 1b**). In addition, a TCF/LEF-dependent TOPFLASH reporter assay revealed that β-catenin transcriptional activity was significantly higher in NMR cells (**Fig. 1c**). These findings imply that the trans-localization of β-catenin into the nucleus and β-catenin signaling is constitutively active in NMR cells. Despite the abundant accumulation of β-catenin in NMR cells, the expression of cyclin D1, a mitogenic factor and primary downstream target of the Wnt/β-catenin pathway, was rather decreased in NMR cells (**Fig. 1a**). Due to lower expression levels of mitogenic factors, NLFs and NSFs grew extremely slowly compared with mouse cells, which exhibited exponential growth (**Fig. 1d**). These unexpected observations suggested unique alterations of β-catenin signaling in NMR cells, and furthermore that this axis could be relevant to the unique attributes of NMR cells.

To investigate whether serum concentration, oxygen concentration and temperature would affect the β-catenin abundance in NMR and mouse cells, I cultured the cell lines at different conditions and confirmed β-catenin expression levels in NSFs were always considerably higher than that of MSFs (**Figures 2**). Interestingly, alignment of β-catenin amino acid sequences highlighted that there is only an amino acid residue difference between human/mouse and NMR β-catenin, indicating that NMR β-catenin is structurally highly conserved among these mammals (**Fig. 3a**)However, β-catenin abundance was not affected by the treatment with IWP2, an inhibitor targeting membrane-bound O-acyltransferase porcupine to prevent Wnt ligand palmitoylation [70], indicating that the accumulation of β-catenin in NMR cells might not occur via autocrine activation of the Wnt signaling **(Fig. 3b)**. Furthermore, overexpression of NMR Axin1 did not decrease β-catenin abundance **(Fig. 3c)**.. These results raise the possibility that β-catenin may have unique functions independent of the canonical Wnt/β-catenin signaling in NMRs.

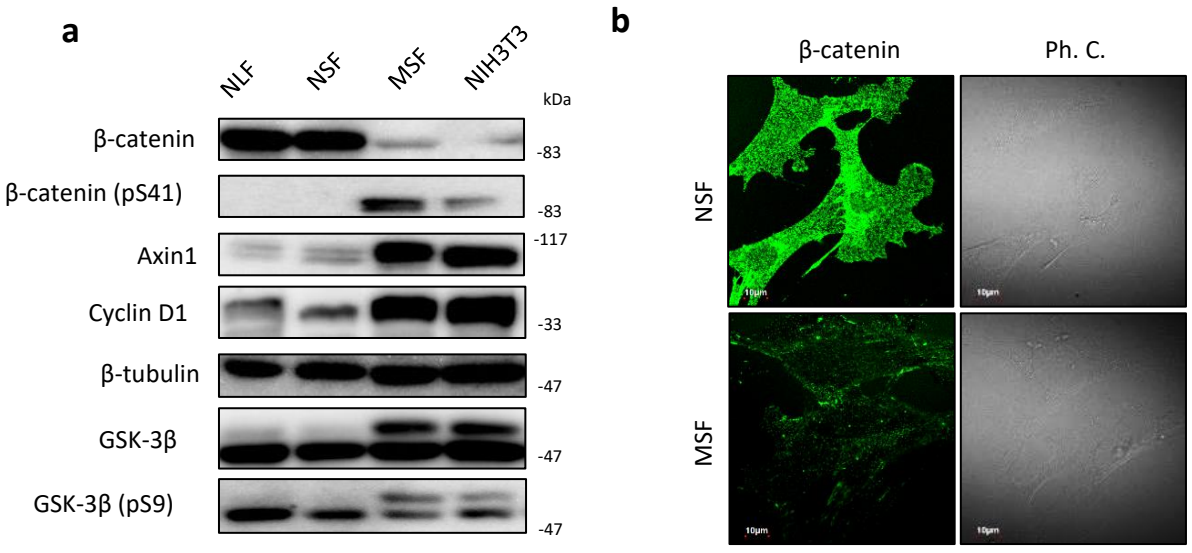

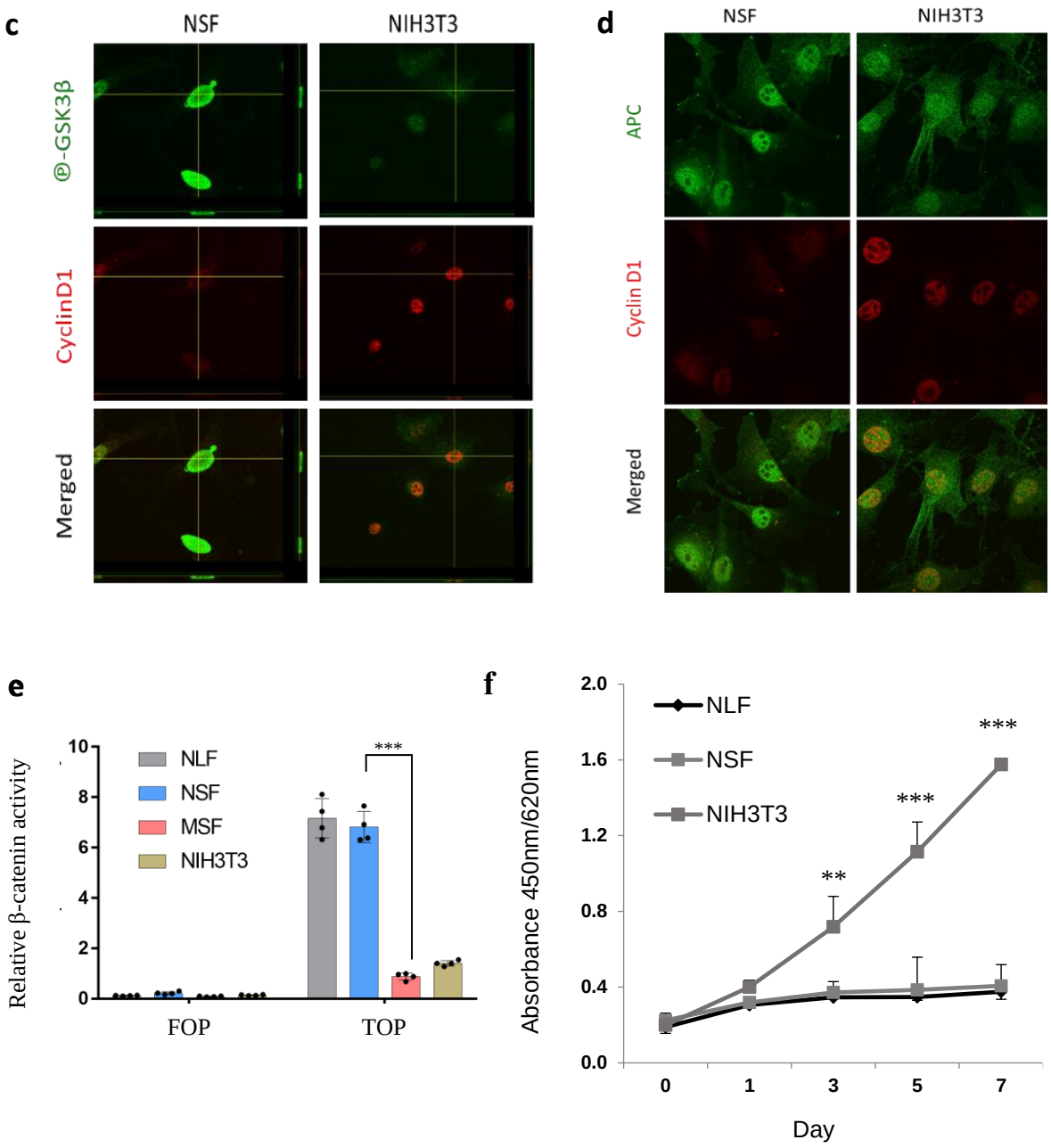

Figure 1. NMR cells exhibit a unique β-catenin signaling. (a) Representative immunoblots comparing expression of β-catenin and its downstream targets in NMR lung fibroblasts (NLFs), NMR skin fibroblasts (NSFs), mouse fibroblasts (MSFs), and NIH 3T3 cells. **(b)** Representative images of immunofluorescence staining of β-catenin in NSFs and MSFs. In the phase-contrast images, unknown microbodies are abundant in NSFs. Immunofluorescence results illustrating the localization and intensity of phosphorylated GSK3β **(c)** and APC **(d)** in NSF and NIH3T3 cells. Scale bar 10μm. **(e)** TOPFLASH reporter assay showing significant differences in relative β-catenin activity between NLFs, NSFs, and NIH 3T3 cells. **(f)** The proliferation rates of NSFs, NLFs, and NIH 3T3 cells were determined in a growth assay conducted for 7 days. Data presented in (c, d) are expressed as the mean ± standard deviation; ***p <0.001, two-sided Student's *t*-test.

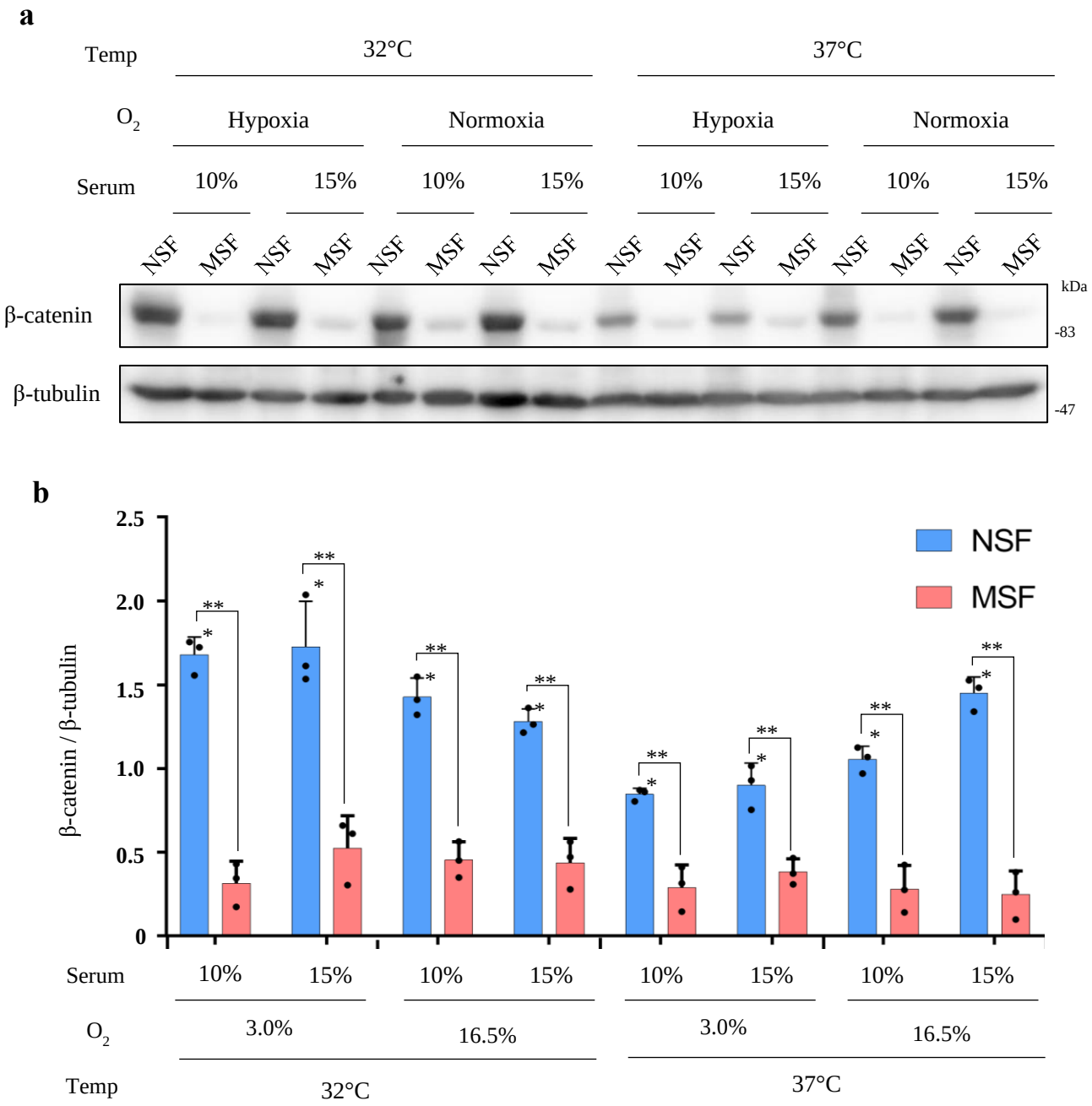

Figure 2. Unique supernumerary accumulation of β-catenin in NMR skin fibroblasts (NSFs). (a) Immunoblot showing that β-catenin expression levels were significantly higher in NSFs than in MSFs. β-tubulin was used as a loading control. **(b)** Densitometric quantification of β-catenin/β-tubulin expression from the immunoblot. Data are expressed as the mean ± standard deviation (n=3 culture wells/group). ***p <0.001, Student's paired *t*-test.

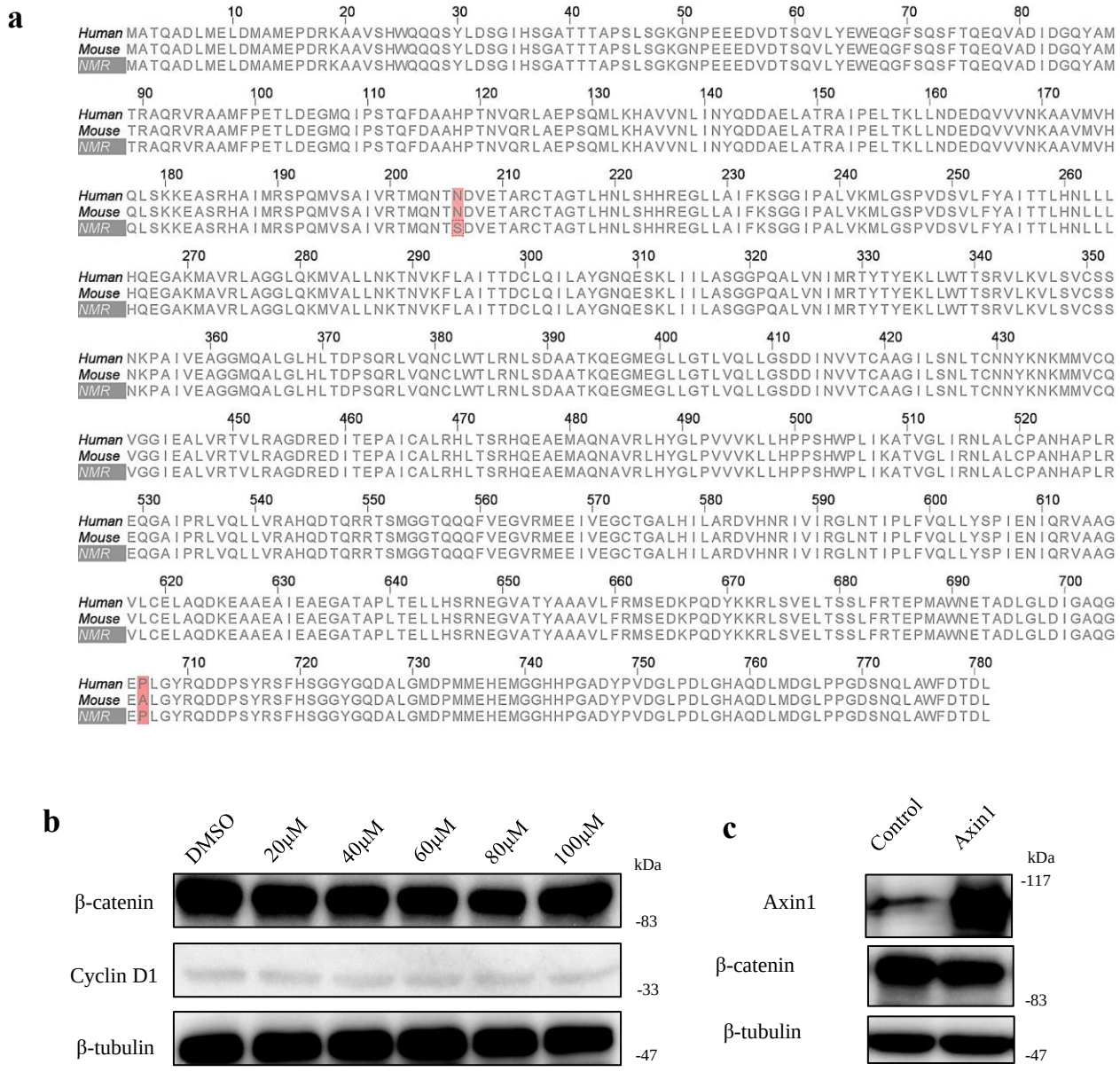

Figure 3. Wnt- and Axin1-independent stabilization of β-catenin accumulation in NSFs. (a) Alignment of the human, mouse, and NMR β-catenin amino acid sequences using Clustal W. **(b)** Immunoblot showing β-catenin expression levels in the presence of increasing doses of IWP-2, an inhibitor of Wnt signaling. β-tubulin was used as a loading control. **(c)** Immunoblot showing that overexpression of the scaffold protein *Axin 1* did not affect changes in β-catenin expression levels observed in NMR cells. β-tubulin was used as a loading control.

3.2 Downregulation of β-catenin induced senescence-like phenotypic changes in NSFs

To identify the functions of β-catenin in NMR cells, we performed shRNA knockdown of β-catenin in NSFs. Immunoblot analysis revealed that β-catenin expression was successfully repressed by β-catenin shRNAs, and concurrently that the expression of cyclin D1 was evidently reduced (**Fig. 4a)**. A TOPFLASH reporter assay also demonstrated that β-catenin knockdown significantly attenuated transcriptional activity [71] (**Fig. 4b**). Phenotypically, β-catenin knockdown resulted in noticeable morphological changes in NSFs, such as increased cell size and cell surface area **(Fig. 4c)**. Furthermore, cell proliferation was markedly decreased in β-catenin-knockdown NSFs **(Fig. 4d)**, indicating that β-catenin still promoted cell proliferation in NSFs. Because the phenotype of β-catenin-knockdown NSFs was similar to that of senescent cells, we measured the activity of senescence-associated-β-galactosidase (SA-β-gal). β-catenin knockdown markedly induced SA-β-gal activation **(Fig. 4e)**. In addition, β-catenin knockdown induced nuclear accumulation of p21, a CDK1 inhibitor used as a marker of cellular senescence **(Fig. 4f)**, and promoted the formation of 8-hydroxy-2'-deoxyguanosine (8-OHdG), a biomarker for DNA damaged by oxidative stress [72,73] **(Fig. 4g)**.

As non-targeting shRNA may target an intended mRNA and induce a stress response within NMR cells, we hereby use the empty vector pLKO1 as the shControl throughout the experiments. Nevertheless, we also included the results comparing β-catenin expression, lipid droplets abundance, and induced-senescence-like phenotypes in NSF shControl, shNon-targeting and shβ-catenin. The induction of SA-β-gal activation and 8-OHdG formation was not affected by the treatment with an empty vector (shControl) or that carrying a non-target shRNA (shNTControl), supporting the specific effects of shRNAs targeting β-catenin (**Fig. 5)**. Taken together, these findings suggested that β-catenin knockdown induced phenotypic changes associated with cellular senescence in NSFs.

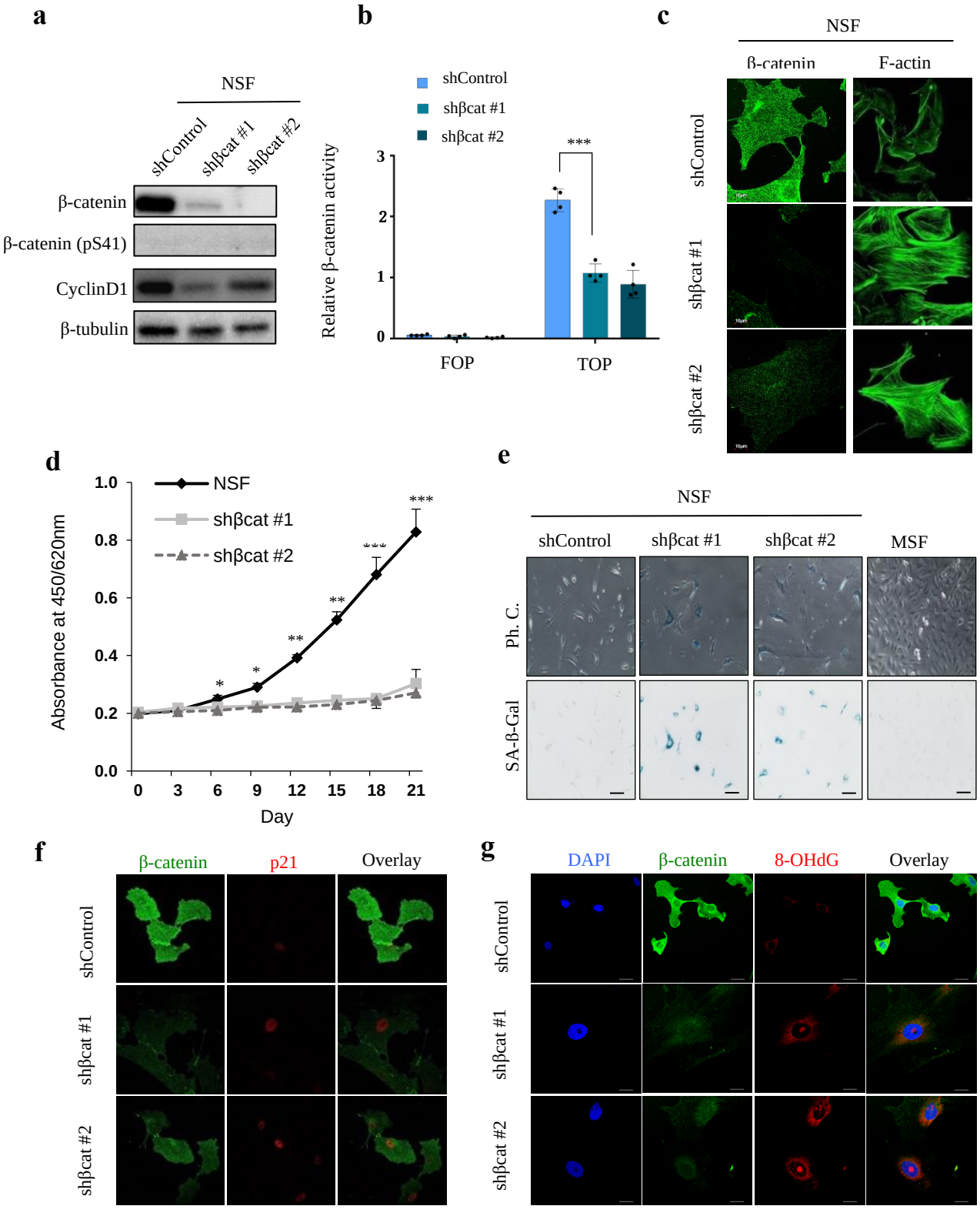

Figure 4. β-catenin knockdown induces senescence-like phenotypic changes in NSFs. (a) Immunoblots showing changes in expression levels of β-catenin pathway after β-catenin knockdown in NSFs. β-tubulin was used as a loading control. (b) TOPFLASH assay showing the relative β-catenin activity of NMR Skin Fibroblasts (NSFs) after the β-catenin knockdown. (c) Morphological changes in NSFs by β-catenin knockdown. Scale bars 10μm. (d) The proliferation rate of NSFs and β-catenin knockdown counterparts were determined by growth assay. Data presented in (b and d) are expressed as mean ± standard deviation (n=4); ***: P<0.001 by Two-sided Student's *t*-test. (e) Representative images showing SA-β-gal activity in control NSF, β-catenin knockdown NSFs, and MSFs (Left). Quantitative analysis of the SA-β-Gal activity in control NSFs, and β-catenin knockdown NSFs (Right). Data presented are expressed as mean ± standard deviation (n=4 culture wells each) (lower graph); ***: P<0.001 by Two-sided Student's *t*-test. (f) Immunofluorescence staining of β-catenin (green) and p21 (red) in NSFs and β-catenin knockdown NSFs. (g) Immunofluorescence staining of β-catenin (green) and 8-OHdG (red) in NSFs and β-catenin knockdown NSFs. Scale bar: 20μm.

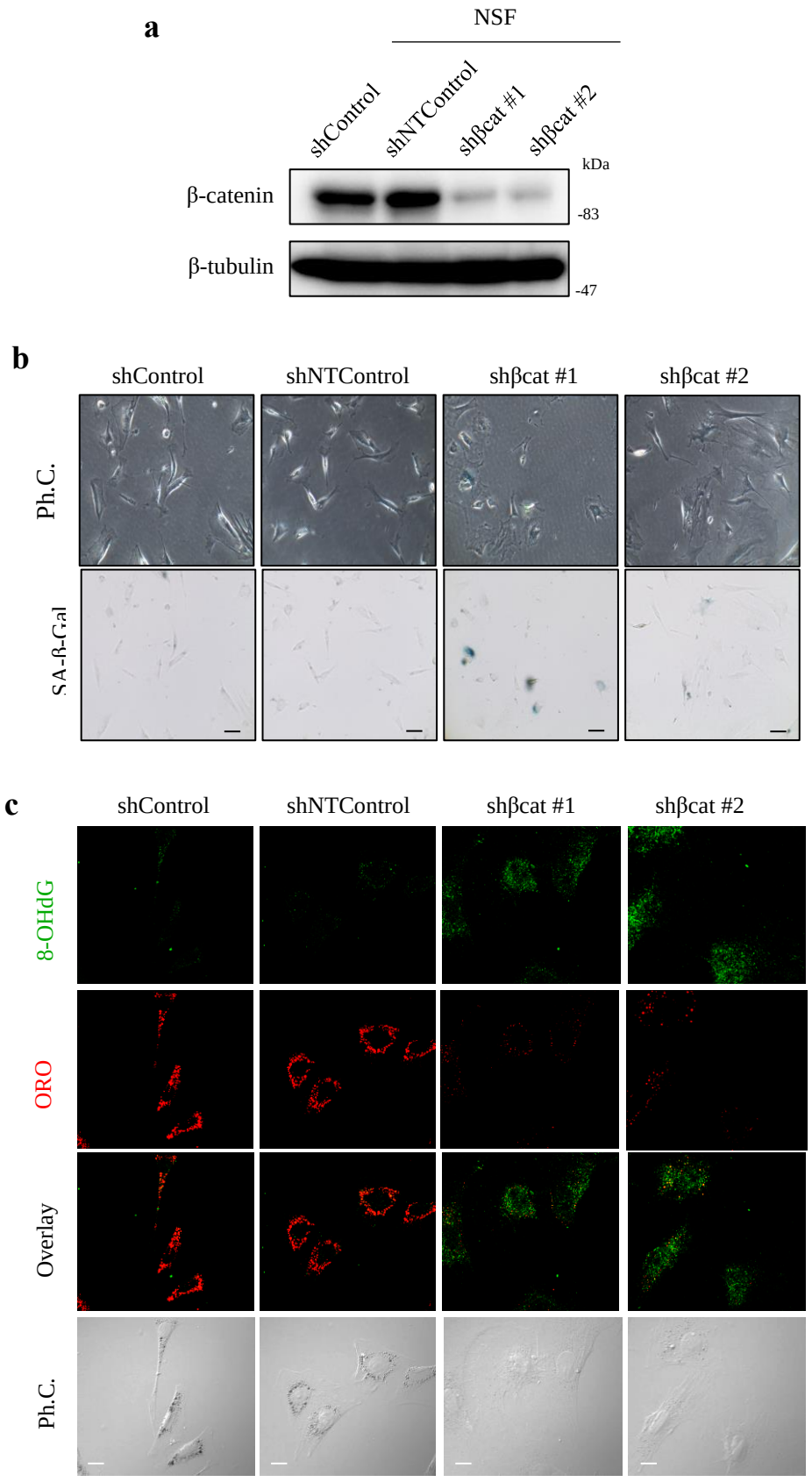

Figure 5: Non-targeting knockdown does not change β-catenin expression or lipid droplet abundance. (a) Immunoblot showing β-catenin expression levels upon treatment with Mock (*shControl*), non-target shRNA (*shNTControl*), and *shβ-catenin*. **(b)** Representative phase-contrast and bright-field images showing SA-β-Gal staining in NSFs treated with *shControl*, *shNTcontrol*, or *shβ-catenin*. Scale bars, 100 μm. **(c)** Immunofluorescence staining of NSFs treated with *shControl*, *shNTcontrol*, and shβ-catenin with 8-OHdG (green) and ORO (red). Scale bars, 20 μm.

3.3 Accumulation of cholesterol-enriched lipid droplets was associated with the abundance of β-catenin

We also observed that NMR cells abundantly accumulated microbodies, which were identified as lipid droplets by oil red O (ORO) staining using two different solvents, 2-propanol and triethyl-phosphate (TEP) (**Fig. 6)**. Quantitative analysis also revealed that NSFs contained lipid droplets more abundantly than MSFs under different cultured conditions (**Fig. 7)**. Since ORO staining with TEP was more sensitive than that with 2-propanol, we hereafter used TEP to stain lipid droplets with ORO (**Fig. 8a)**. Transmission electron microscopy (TEM) further confirmed that round-shaped lipid droplets were more abundant in NSFs than in NIH 3T3 cells (**Fig. 8b**). Interestingly, we found that lipid droplet formation was abolished by β-catenin knockdown in NSFs **(Fig. 8c)**, suggesting a functional link between lipid droplet formation and β-catenin-mediated senescence-like phenotypic changes.

To explore this possibility, we analyzed the contents of NSF lipid droplets. Quantitative analysis of triglycerides, one of the lipid droplet component, were comparable between NSFs and MSFs (**Fig. 9a**). Contrastingly, quantitative analysis of total cholesterol contents revealed that cholesterol was more abundant in NSFs than in MSFs, which was also significantly decreased by β-catenin knockdown (**Figure 10a**). These results suggested that lipid droplets in NSFs were comprised primarily of cholesterol rather than triglycerides. The contribution of cholesterol to β-catenin-dependent lipid droplet was further examined using CholEsteryl BODIPY FL C_{12}, a tracer of cholesterol transport. The fluorescence analysis showed that cholesterol transport into ORO-positive lipid droplets in NSFs was inhibited by β-catenin knockdown (**Fig. 10b**), implying that β-catenin signaling may be involved in the regulation of cholesterol transport.

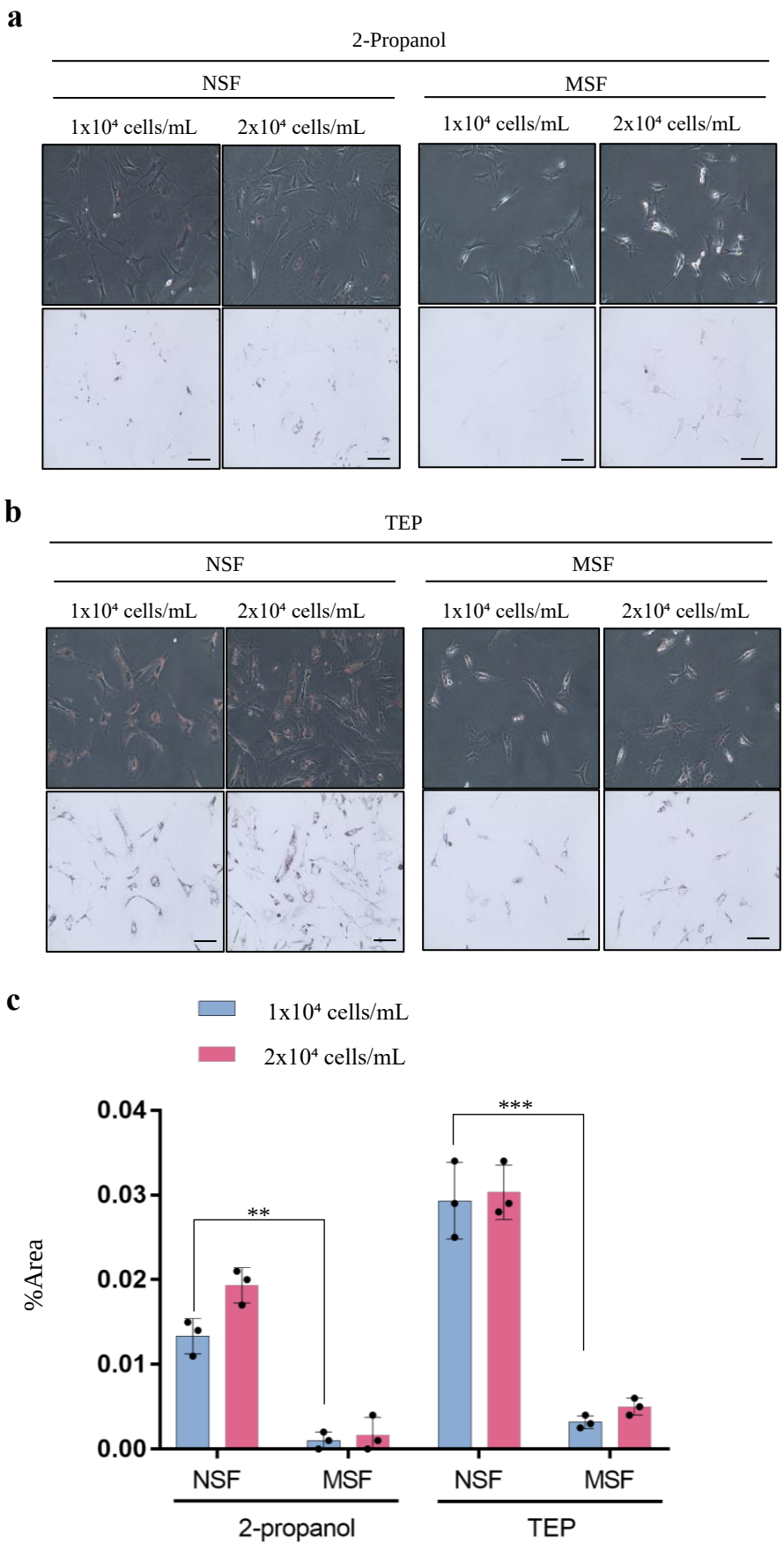

Figure 6. Comparison of staining of lipid droplets using Isopropanol and Triethyl phosphate. Representative bright-field images showing lipid droplet staining by ORO in NSFs (a) and MSFs (b) under the indicated conditions. Scale bars, 100 µm. **(c)** Quantitative analysis of ORO-stained NSFs and MSFs under the indicated conditions. The ratio of the stained area to the total area was analysed with Image J software. Data are expressed as the mean ± standard deviation (n=3 culture wells/group). **p<0.01 and ***p<0.001, Student's paired *t*-test.

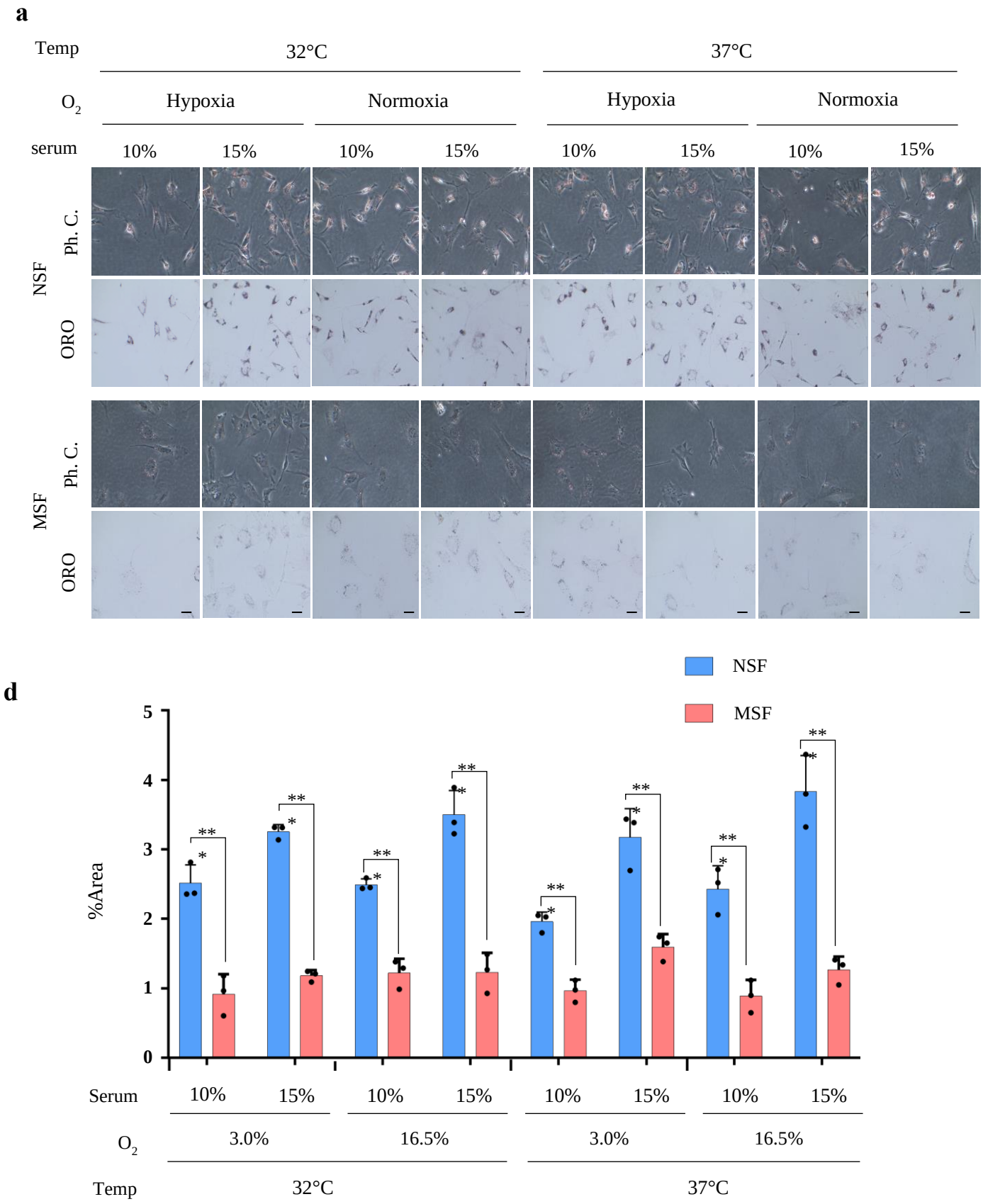

Figure 7. Lipid droplets accumulate in NSFs, regardless of culture conditions. (a) Representative images showing that stained lipid droplets were significantly more abundant in NSFs than in MSFs under different culture conditions. **(b)** Quantitative results (obtained using ImageJ software) showing percentage coverage of cells stained with ORO over that by total cells. Scale bars, 100 μm. Data are expressed as the mean ± standard deviation (n=3 culture wells/group). ***p<0.001, Student's unpaired *t*-test.

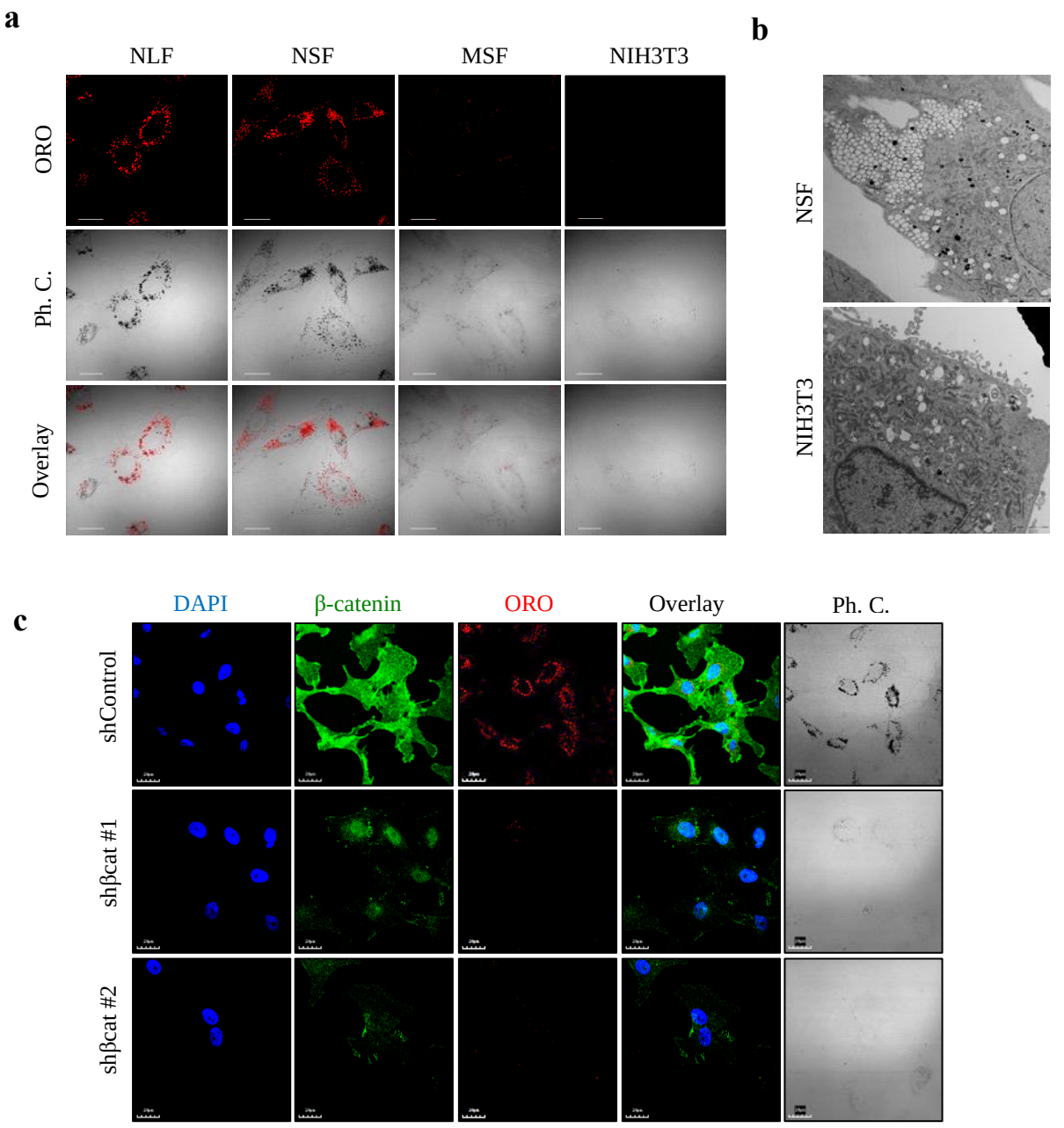

Figure 8. Association between β-catenin abundance and lipid droplet accumulation. (a) Representative confocal images showing staining of lipid droplets by ORO in NLFs, NSFs, MSFs, and NIH 3T3 cells. Scale bar, 20 μm. **(b)** Representative TEM images showing robust lipid droplet accumulation in NSFs. Scale bar, 5 μm. **(c)** Representative fluorescence images of DAPI, β-catenin, and ORO staining, along with phase-contrast images, of control and *β-catenin* knockdown NSFs. Scale bar, 20 μm.

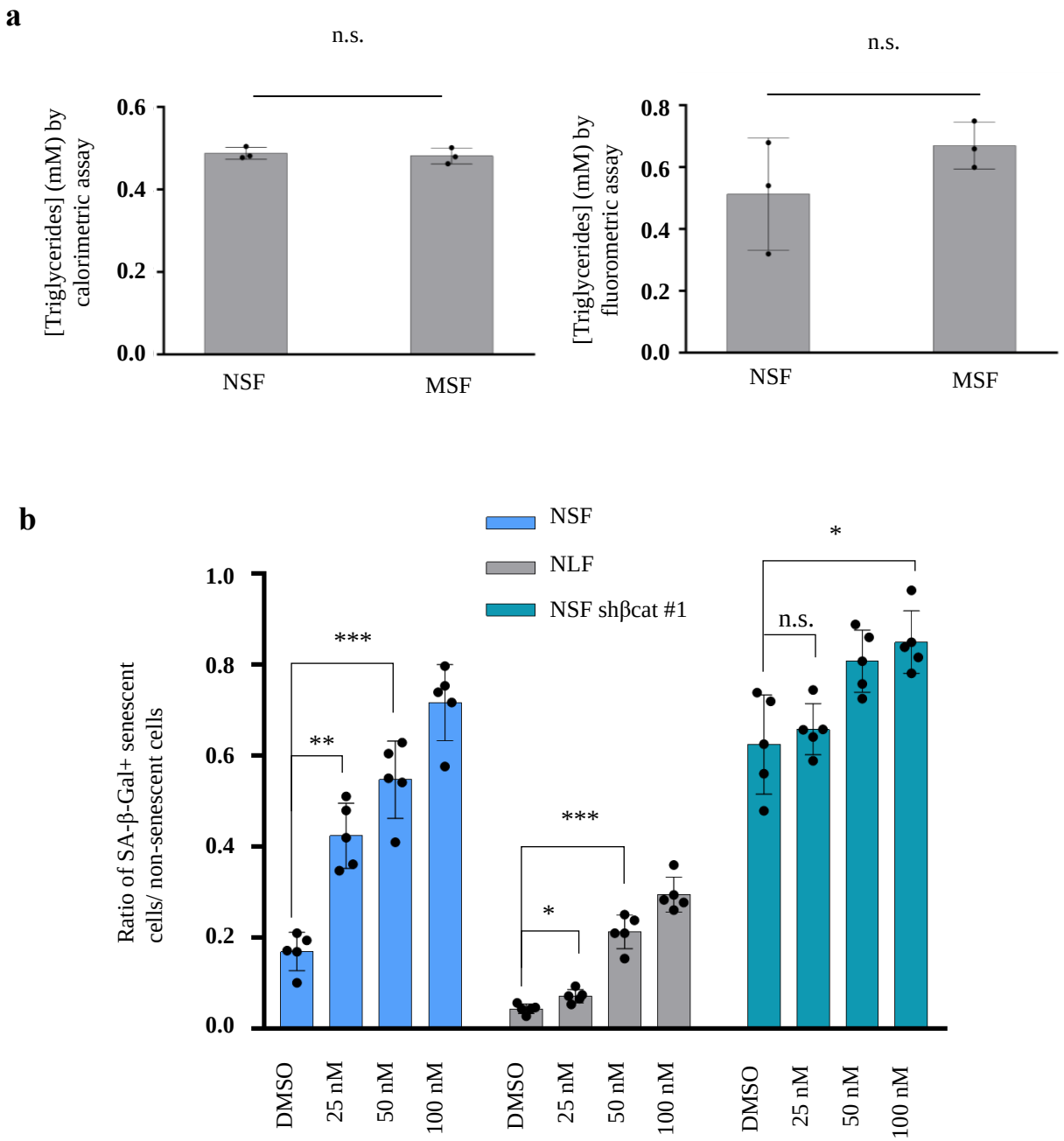

Figure 9. NMR cells accumulate lipid droplets consisting primarily of cholesterol. (a) Colorimetric (left) and fluorometric (right) assays comparing triglyceride concentrations between NSFs and MSFs. Data are expressed as the mean ± standard deviation (n=3 culture wells/group). n.s, non-significant, Student's unpaired *t*-test . **(b)** Quantitative analysis of SA-β-Gal-stained cells in control NSFs and NLFs, and *β-catenin* knockdown NSFs, which were treated with the indicated concentrations of lovastatin. Data are expressed as the mean ± standard deviation (n=5 culture wells/group). n.s, non-significant; *P<0.05, **P<0.01, and ***P<0.001, Student's unpaired *t*-test.

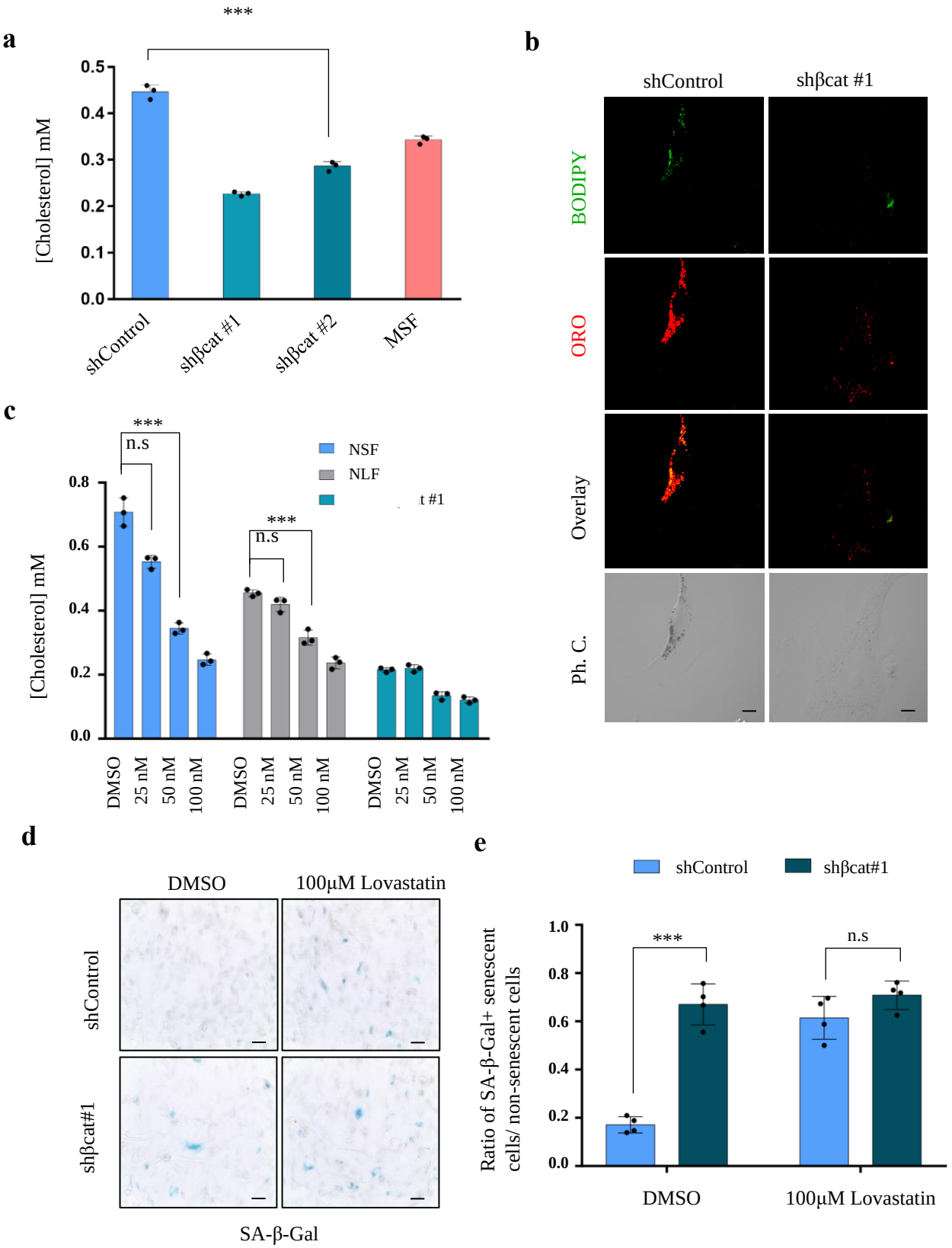

Figure 10. Association between senescence-like phenotypes and accumulation of cholesterol-enriched lipid droplets. (a) Representative confocal images showing staining of cholesteryl ester by BODIPY C12 in NSF *shControl* and *shβ-catenin* cells, with or without serum. Scale bar, 20 μm. **(b)** Cholesterol assay demonstrating that *β-catenin* knockdown decreases the cholesterol concentration. **(c)** The cholesterol concentration was decreased by lovastatin treatment in a dose-dependent manner. Data are expressed as the mean ± standard deviation (n=3 culture wells/group); ***P<0.001, two-sided Student's *t*-test. **(d)** Representative bright-field images showing that inhibition of cholesterol synthesis in NSFs increases SA-β-gal activity. **(e)** Quantitative analysis of SA-β-Gal-stained cells in control and *β-catenin* knockdown NSFs. Data are expressed as the mean ± standard deviation (n=4 culture wells/group); ***P<0.001, two-sided Student's *t*-test.

To assess the physiological relevance of cholesterol-enriched lipid droplets in NSFs, we examined the effects of cholesterol synthesis inhibition on cellular phenotypes. Treatment of NSFs with lovastatin, an HMG-CoA reductase inhibitor, decreased cellular cholesterol contents in a dose-dependent manner to a level equivalent to that of β-catenin knockdown cells (**Fig. 10c**). Under cholesterol inhibition, NSFs exhibited SA-β-gal activation, as in β-catenin knockdown cells (**Fig. 9b and Fig. 10d,e)**. These findings suggested that cholesterol was crucial for protecting NMR cells from senescence-like phenotypic changes.

To further examine if the phenotypic changes induced by β-catenin knockdown in NMR cells were indeed due to cellular senescence, NSFs were treated with the DNA cross-linking agent mitomycin C to induce therapy-induced senescence. Treatment of NSFs with mitomycin C increased SA-β-gal activity to a level similar to that of β-catenin knockdown NSFs (**Fig. 11a, b)**. Mitomycin C treatment also induced nuclear p21 accumulation, although it did not affect lipid droplet formation (**Fig. 11c**). Furthermore, treatments involved 48-hour incubation in the culture medium with 10μg/mL cholesterol:β-cyclodextrin (C4951, Sigma) [67,68] in β-catenin knockdown senescent-like cells failed to suppress the induction of SA-β-gal activity, indicating that the cellular events induced by β-catenin knockdown were irreversible (**Fig. 12**). These observations demonstrated that the phenotypic changes induced by β-catenin knockdown and/or cholesterol depletion were tightly associated with cellular senescence.

As cumulative population doubling could increase SA-β-Gal activity [74,75] and lipid droplets are widely distributed in aged cells [76,77], we performed ORO staining of NSFs at different passage numbers to determine if NMR cells accumulated lipid droplets as replicative senescence progress. Lipid droplet abundance was unchanged irrespective of passage number (**Fig. 13**), corroborating that supernumerary lipid droplets in NSFs were a unique feature of NMR cells.

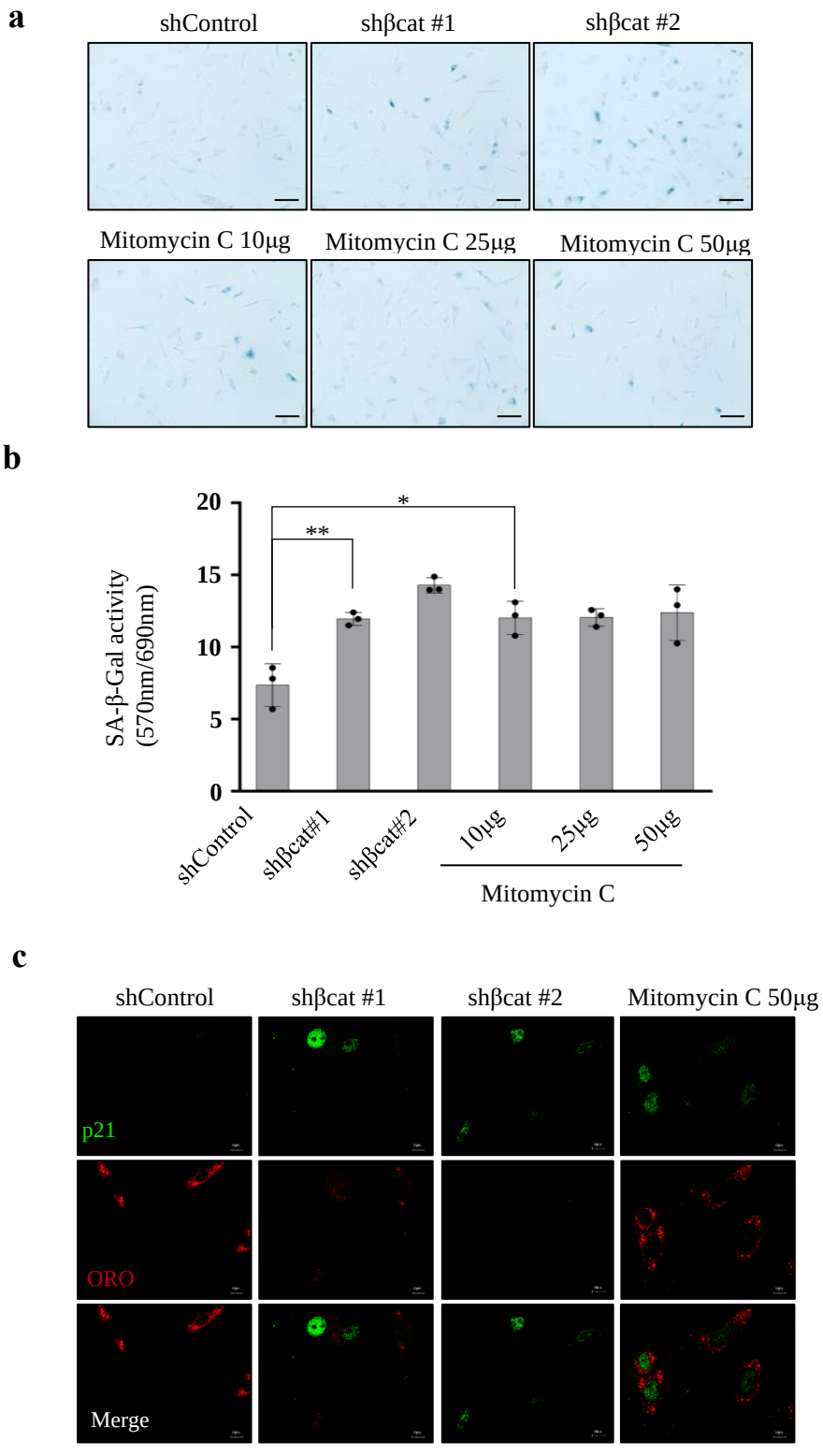

Figure 11. NSF lipid droplet formation was not affected by therapy-induced senescence. (a) SA-β-Gal assay in NSFs demonstrating induction of senescence by Mitomycin C. Scale bar, 100 µm. **(b)** CPRG assay quantifying SA-β-Gal activity in NSFs upon Mitomycin C treatment. Data are expressed as the mean ± standard deviation (n=3 culture wells/group). * P<0.05 and **p<0.01, Student's unpaired *t*-test. **(c)** Expression of p21 (green) and staining of lipid droplets (red) were observed by confocal microscopy of NSFs subjected to Mitomycin C treatment. Scale bars, 10 µm.

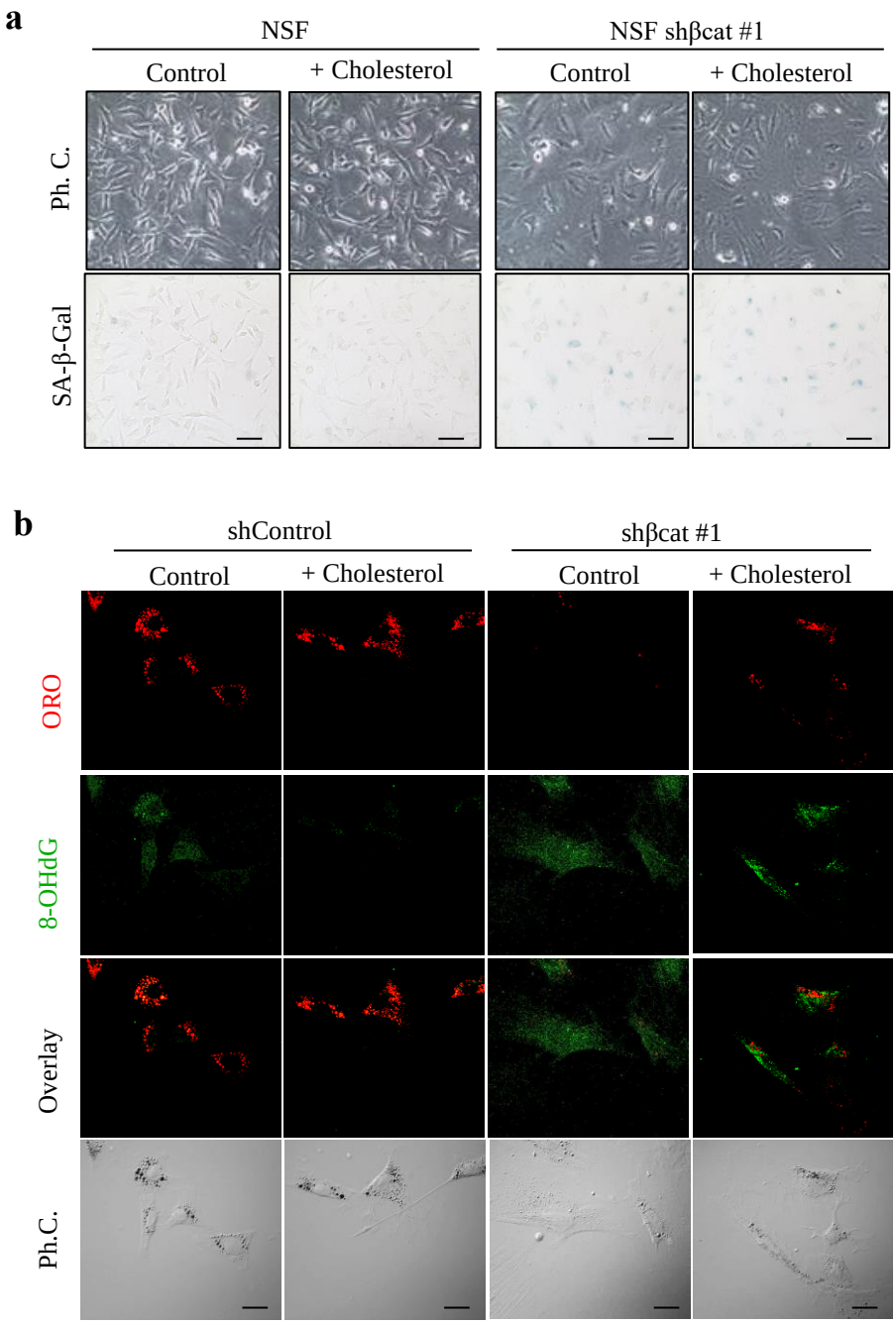

Supplemental Figure 12. Cholesterol loading fails to protect NSFs from cellular senescence under *β-catenin* knockdown conditions. (a) Representative images of SA-β-Gal activity in control NSFs and *β-catenin* knockdown NSFs with or without cholesterol loading. Scale bars, 100 μm. **(b)** Immunofluorescence staining of 8-OHdG (green) and ORO (red) in NSFs and β-catenin knockdown NSFs with or without cholesterol loading (10 μg/mL). Scale bars, 20 μm.

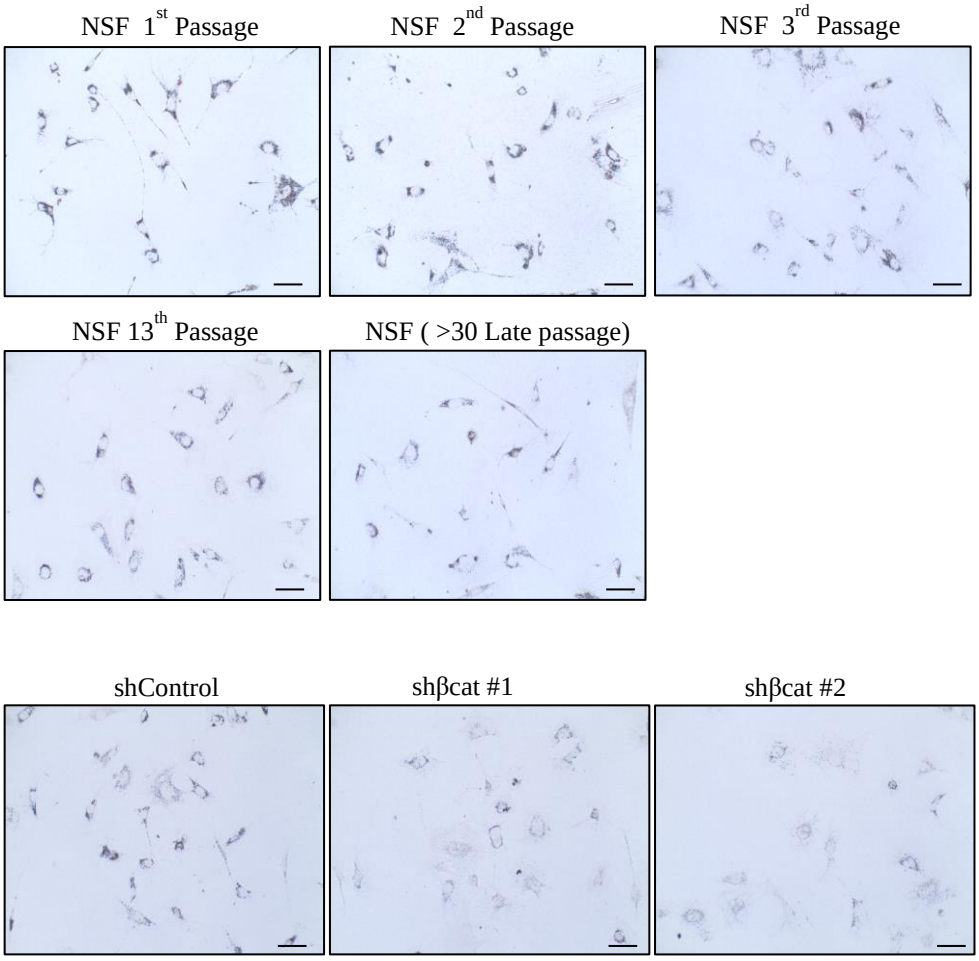

Figure 13. Lipid droplet abundance in NSFs is unaffected by passage number. Representative bright-field images showing staining of lipid droplets by ORO in control NSFs at different passages and *β-catenin* knockdown NSFs as a negative control. Scale bars, 100 μm.

3.4 β-catenin abundance was closely associated with the LXR/RXR pathway in NMR cells

To determine the mechanisms by which β-catenin induced accumulation of cholesterol-enriched lipid droplets, we performed comparative RNA-seq analysis of control and β-catenin knockdown NSFs. Raw RNA-seq data was submitted under Gene Expression Omnibus (GEO) accession number GSE147871. Ingenuity Pathway Analysis (IPA) revealed that the LXR/RXR pathway, which modulates cholesterol metabolism and lipogenesis, was significantly downregulated by β-catenin knockdown **(Fig. 14)**. Among the genes involved in the LXR/RXR pathway, only apolipoprotein F (ApoF), a secreted glycoprotein that associates with LDL/HDL, was prominently downregulated by β-catenin knockdown (**Fig. 14 and Supplementary Table 1**), which was corroborated by RT-PCR analysis (**Fig. 14b**). ApoF inhibits cholesteryl ester transfer protein (CETP)-mediated cholesterol transfer between lipoproteins [78-82] (**Fig. 14c**). Therefore, the upregulation of ApoF in NMRs likely suppresses the transfer of cholesterol among lipoproteins, which might contribute to the accumulation of cholesterol in lipid droplets. As a consequence of the suppression of the LXR/RXR pathway by β-catenin knockdown, NF□B was activated to upregulate its downstream targets, such as IL1B, MMP2, MSR1, and NOS2 (**Fig. 14e and Supplementary Table 2**). These findings suggested that the accumulation of lipid droplets in NSFs was attributable to the activation of the LXR/RXR pathway via the upregulation of ApoF.

3.5 ApoF knockdown mimicked the effects of β-catenin knockdown in NSFs

To verify the role of ApoF in the β-catenin signaling in NMRs, we then proceeded with the genetic ablation of ApoF in NSFs. The expression of ApoF protein was successfully suppressed by shApoF as well as shβcat (**Fig. 15a, b and Fig. 16a**). ApoF knockdown significantly induced suppression of ORO-positive lipid droplet formation (**Fig. 15c**) and promoted activation of SA-β-gal (**Fig. 15d**). These findings indicated that ApoF knockdown could mimic the effects of β-catenin knockdown in NSFs, suggesting that ApoF plays roles downstream of the β-catenin signaling.

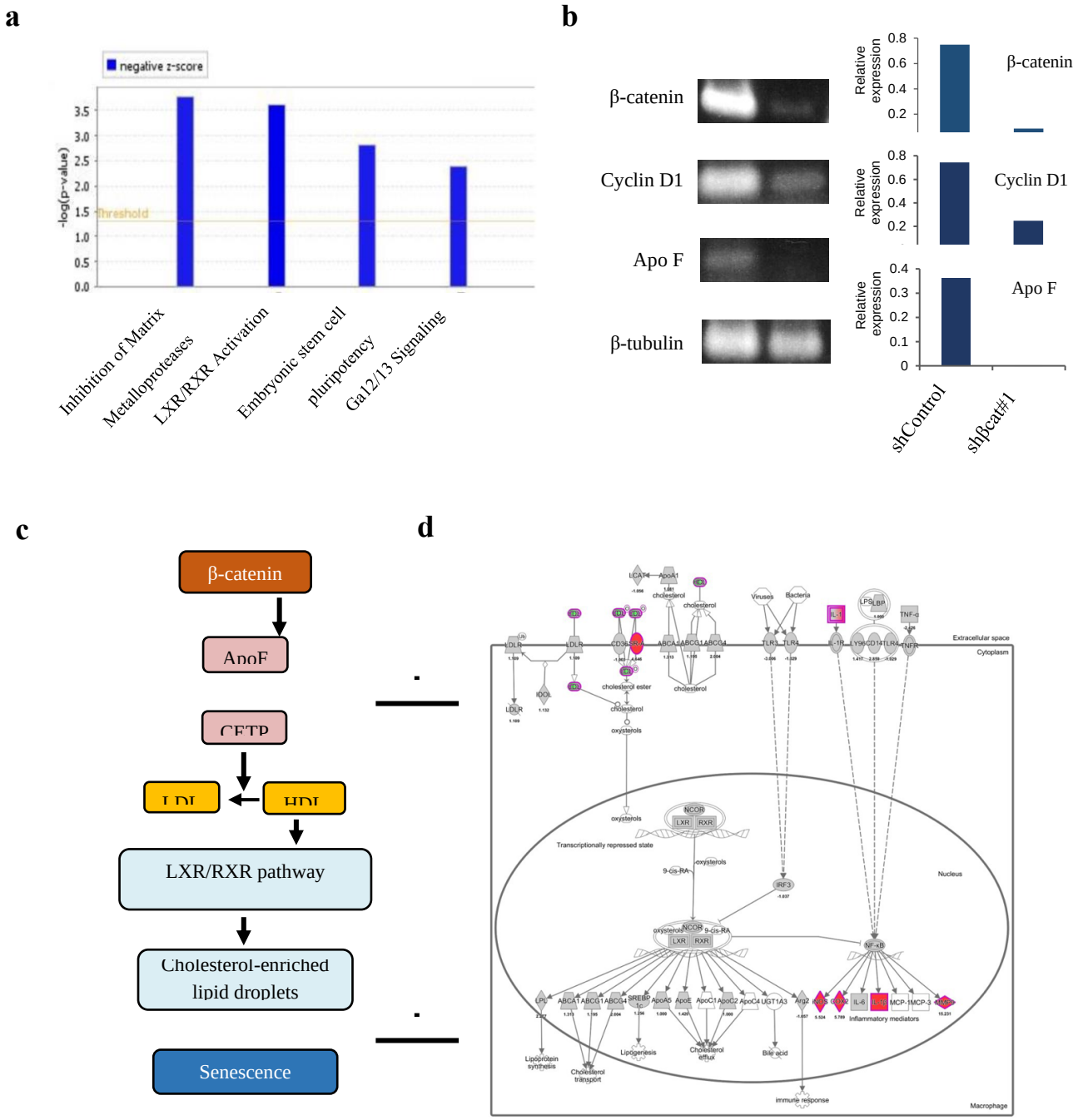

Figure 14. Association between β-catenin abundance and LXR/RXR activation in NSFs. (a) Ingenuity Pathway Analysis (IPA) results showing pathways that were significantly affected (>4-fold-change) by *β-catenin* knockdown in NSFs. **(b)** Genes showing significant expression changes in *β-catenin* knockdown conditions. **(c)** Analysis of target genes regulated by β-catenin in NSFs by RT-PCR (left panels). Quantitative data are also shown (right-most graphs). **(d)** Schematic diagram illustrating potential links between β-catenin, ApoF, the LXR/RXR pathway, cholesterol biosynthesis and metabolism, lipid droplets, and senescence in NMR cells. **(d)** Schematic IPA diagrams showing LXR/RXR-dependent changes in gene expression potentiated by *β-catenin* knockdown.

Supplemental Table 1. Representative downregulated genes within DEG from RNA-seq

Fold Change	gene name	Description
-13.584	Wnt10b	Wnt family member 10B
-12.199	Lpar3	lysophosphatidic acid receptor 3
-11.079	LOC110345950	uncharacterized LOC110345950
-10.307	Fam220a	family with sequence similarity 220 member A
-8.317	LOC101716611	uncharacterized LOC101716611
-7.796	Eln	elastin
-7.686	Ctnnb1	catenin beta 1
-7.656	Mxi1	"MAX interactor 1, dimerization protein"
-7.334	Cavin2	caveolae associated protein 2
-6.376	Cpxm1	"carboxypeptidase X, M14 family member 1"
-6.322	Fam198a	Golgi Associated Kinase 1A
-6.191	Efhd1	EF-hand domain family member D1
-5.845	LOC110348574	uncharacterized LOC110348574
-5.826	Entpd3	ectonucleoside triphosphate diphosphohydrolase 3
-5.822	LOC101725231	60S ribosomal protein L9 pseudogene
-5.822	LOC110346661	uncharacterized LOC110346661
-5.822	LOC106010386	uncharacterized LOC106010386
-5.822	LOC101710023	uncharacterized LOC101710023
-5.822	LOC106008187	uncharacterized LOC106008187
-5.813	Trerf1	transcriptional regulating factor 1
-5.715	Ano1	anoctamin 1
-5.452	Dlk2	delta like non-canonical Notch ligand 2
-5.446	Ankrd29	ankyrin repeat domain 29
-5.406	Sox2	SRY-box 2
-5.120	Egfl6	EGF like domain multiple 6
-4.991	LOC110348191	uncharacterized LOC110348191
-4.990	LOC101717878	myc-associated zinc finger protein pseudogene
-4.990	LOC110346939	zinc finger protein 670 pseudogene
-4.990	LOC110346980	gametocyte-specific factor 1 pseudogene
-4.990	LOC110350373	uncharacterized LOC110350373
-4.990	LOC101711524	transcriptional coactivator YAP1 pseudogene
-4.990	LOC110347540	uncharacterized LOC110347540
-4.981	Efcab1	EF-hand calcium binding domain 1
-4.713	Pi15	peptidase inhibitor 15
-4.671	Map2k6	mitogen-activated protein kinase kinase 6
-4.614	Morn5	MORN repeat containing 5
-4.574	LOC110350023	uncharacterized LOC110350023
-4.574	LOC101718238	protein AF-9-like
-4.574	LOC110348851	uncharacterized LOC110348851
-4.395	S1pr5	sphingosine-1-phosphate receptor 5
-4.366	LOC110345400	E3 ubiquitin-protein ligase HACE1-like
-4.348	Cgnl1	cingulin like 1
-4.347	LOC101712708	uncharacterized LOC101712708
-4.325	LOC101707839	cadherin-18
-4.286	LOC101704034	"UDP-GalNAc:beta-1,3-N-acetylgalactosaminyltransferase 1-like"
-4.282	Ctnna2	catenin alpha 2
-4.268	Fuca2	alpha-L-fucosidase 2
-4.256	Peg10	paternally expressed 10
-4.158	LOC106009933	ras-related protein Rab-5A-like
-4.158	Apof	apolipoprotein F
-4.158	LOC110347698	eukaryotic translation initiation factor 4E pseudogene
-4.158	LOC101712597	cyclin-dependent kinase 1 pseudogene
-4.158	LOC101718707	small integral membrane protein 19 pseudogene
-4.158	Mylpf	"myosin light chain, phosphorylatable, fast skeletal muscle"
-4.158	LOC106009357	vesicle transport protein GOT1B-like
-4.158	LOC101712679	40S ribosomal protein SA pseudogene
-4.158	LOC101707806	intercellular adhesion molecule 3
-4.158	CUNH10orf10	DEPP1 Autophagy regulator
-4.006	Serpinb7	serpin family B member 7

Supplemental Table 2. Representative upregulated genes within DEG from RNA-seq

Fold Change	gene name	Description	Fold Change	gene name	Description
4.008	LOC101696494	UDP-glucuronosyltransferase 1-9-like	5.210	LOC106010809	translationally-controlled tumor protein pseudogene
4.008	LOC101708467	U5 small nuclear ribonucleoprotein 40 kDa protein pseudogene	5.210	Plet1	placenta expressed transcript 1
4.008	Rasd1	ras related dexamethasone induced 1	5.215	LOC101723772	uncharacterized LOC101723772
4.008	Gpr15	G protein-coupled receptor 15	5.221	LOC101725671	T-complex protein 1 subunit zeta
4.014	Sycp1	synaptonemal complex protein 1	5.284	LOC110344690	uncharacterized LOC110344690
4.016	Prr15	proline rich 15	5.291	LOC106008440	uncharacterized LOC106008440
4.029	LOC110344797	uncharacterized LOC110344797	5.410	LOC110347960	uncharacterized LOC110347960
4.030	LOC101707377	alveolar macrophage chemotactic factor	5.411	Ido1	"indoleamine 2,3-dioxygenase 1"
4.033	LOC106008493	uncharacterized LOC106008493	5.411	LOC110344930	uncharacterized LOC110344930
4.058	LOC110345612	uncharacterized LOC110345612	5.411	LOC101724224	uncharacterized LOC101724224
4.070	Spock2	"SPARC (osteonectin), cwcv and kazal like domains proteoglycan 2"	5.427	Scg2	secretogranin II
4.133	Cldn34	claudin 34	5.438	Gjb2	gap junction protein beta 2
4.162	Gabbr2	gamma-aminobutyric acid type B receptor subunit 2	5.475	LOC110344528	uncharacterized LOC110344528
4.169	Mest	mesoderm specific transcript	5.581	Lancl3	LanC like 3
4.169	CUNH15orf48	chromosome unknown C15orf48 homolog	5.599	Hsd11b1	hydroxysteroid 11-beta dehydrogenase 1
4.183	LOC110345861	uncharacterized LOC110345861	5.611	LOC110348594	40S ribosomal protein S2 pseudogene
4.207	LOC110344733	uncharacterized LOC110344733	5.621	Hdac9	histone deacetylase 9
4.208	LOC110350140	uncharacterized LOC110350140	5.688	Cited1	Cbp/p300 interacting transactivator with Glu/Asp rich carboxy-terminal domain 1
4.208	LOC101699425	hippocampus abundant transcript-like protein 1 pseudogene	5.711	LOC110347419	uncharacterized LOC110347419
4.208	Lyg1	lysozyme g1	5.772	LOC101698282	uncharacterized LOC101698282
4.212	Dfna5	Non-sybdromic hearing impariment protein 5	5.789	Ptgs2	prostaglandin-endoperoxide synthase 2
4.214	LOC110344645	uncharacterized LOC110344645	5.877	Svep1	"sushi, von Willebrand factor type A, EGF and pentraxin domain containing 1"
4.231	Mcf2l2	MCF.2 cell line derived transforming sequence-like 2	6.012	LOC110348319	uncharacterized LOC110348319
4.255	Scarf1	scavenger receptor class F member 1	6.012	Capns2	calpain small subunit 2
4.303	Fam83e	family with sequence similarity 83 member E	6.012	LOC101698865	eotaxin
4.316	Plg	plasminogen	6.012	LOC101701394	ADP-ribosylation factor-like protein 2-binding protein pseudogene
4.329	LOC110345217	uncharacterized LOC110345217	6.012	LOC110351010	histone H3
4.335	LOC110344203	uncharacterized LOC110344203	6.012	LOC110344276	uncharacterized LOC110344276
4.348	LOC101698571	uncharacterized LOC101698571	6.012	Foxa1	forkhead box A1
4.358	LOC101701112	histone-lysine N-methyltransferase PRDM9	6.012	LOC101702235	ferritin light chain pseudogene
4.383	Gtsf1	gametocyte specific factor 1	6.054	Hck	"HCK proto-oncogene, Src family tyrosine kinase"
4.391	LOC110345541	uncharacterized LOC110345541	6.105	Rgcc	regulator of cell cycle
4.409	LOC110347769	translation initiation factor IF-2-like	6.168	Syn1	synapsin I
4.409	LOC110344201	uncharacterized LOC110344201	6.195	Acpp	"acid phosphatase, prostate"
4.409	Podxl2	podocalyxin like 2	6.456	Col28a1	collagen type XXVIII alpha 1 chain
4.409	LOC101696562	uncharacterized LOC101696562	6.613	Scg5	secretogranin V
4.482	Zfyve28	zinc finger FYVE-type containing 28	6.633	Gjb6	gap junction protein beta 6
4.486	LOC110349692	uncharacterized LOC110349692	6.814	Cldn16	claudin 16
4.493	LOC101706767	platelet basic protein-like	6.914	LOC110344990	uncharacterized LOC110344990
4.500	CUNH2orf81	chromosome unknown C2orf81 homolog	6.919	Olfm4	olfactomedin 4
4.529	Sla	Src like adaptor	7.214	LOC110344566	uncharacterized LOC110344566
4.542	Rassf10	Ras association domain family member 10	7.214	LOC101715086	uncharacterized LOC101715086
4.609	Thy1	Thy-1 cell surface antigen	7.214	LOC110346404	uncharacterized LOC110346404
4.620	Cfap126	cilia and flagella associated protein 126	7.214	LOC106009632	uncharacterized LOC106009632
4.646	Msr1	macrophage scavenger receptor 1	7.214	LOC106010244	60S ribosomal protein L17 pseudogene
4.659	Kcnn3	potassium calcium-activated channel subfamily N member 3	7.338	Pamr1	peptidase domain containing associated with muscle regeneration 1
4.750	Tnip3	TNFAIP3 interacting protein 3	7.522	Nrg2	neuregulin 2
4.810	Kcnab1	potassium voltage-gated channel subfamily A member regulatory beta subunit 1	7.666	Dcn	decorin
4.810	LOC110348315	uncharacterized LOC110348315	7.808	Ccdc141	coiled-coil domain containing 141
4.810	LOC110345795	uncharacterized LOC110345795	7.816	LOC101714691	uncharacterized LOC101714691
4.810	LOC110347917	uncharacterized LOC110347917	7.816	LOC110346356	uncharacterized LOC110346356
4.810	LOC101701625	nascent polypeptide-associated complex subunit alpha pseudogene	7.824	Cp	ceruloplasmin
4.810	LOC110348910	uncharacterized LOC110348910	8.237	LOC110348169	uncharacterized LOC110348169
4.810	LOC101709453	growth hormone-inducible transmembrane protein pseudogene	8.331	LOC101705012	"HLA class II histocompatibility antigen, DRB1-4 beta chain"
4.810	LOC110344130	uncharacterized LOC110344130	8.417	Pdzk1ip1	PDZK1 interacting protein 1
4.810	LOC110347252	uncharacterized LOC110347252	8.417	LOC110348227	uncharacterized LOC110348227
4.810	LOC110349696	uncharacterized LOC110349696	8.417	LOC110344608	uncharacterized LOC110344608
4.810	LOC110347215	uncharacterized LOC110347215	8.417	LOC110350948	uncharacterized LOC110350948
4.810	Ptprh	protein tyrosine phosphatase receptor type H	8.417	LOC110350012	uncharacterized LOC110350012
4.810	LOC110349749	histone H4	8.417	LOC110346739	uncharacterized LOC110346739
4.810	LOC110343935	uncharacterized LOC110343935	9.379	LOC110344368	uncharacterized LOC110344368
4.810	LOC101721253	uncharacterized LOC101721253	9.619	LOC110345873	uncharacterized LOC110345873
4.810	Cspg5	chondroitin sulfate proteoglycan 5	9.619	LOC110345817	protein FAM177A1 pseudogene
4.813	LOC110346620	uncharacterized LOC110346620	9.672	Ccl20	C-C motif chemokine ligand 20
4.854	LOC110347520	uncharacterized LOC110347520	9.943	Rab11fip4	RAB11 family interacting protein 4
4.954	LOC106007905	uncharacterized LOC106007905	10.268	LOC101718744	plasminogen activator inhibitor 2
5.017	LOC110350177	uncharacterized LOC110350177	10.462	Cd74	CD74 molecule
5.034	Ehf	ETS homologous factor	10.822	LOC110351111	uncharacterized LOC110351111
5.091	Mmp8	matrix metallopeptidase 8	11.183	Il21r	interleukin 21 receptor
5.110	LOC110350464	uncharacterized LOC110350464	13.055	Fdcsp	follicular dendritic cell secreted protein
5.110	LOC101721336	uncharacterized LOC101721336	13.151	LOC101704667	"HLA class II histocompatibility antigen, DQ alpha 1 chain"
5.124	LOC101712048	serum amyloid A-4 protein	13.646	Selp	selectin P
5.129	LOC106007907	uncharacterized LOC106007907	13.948	Il1b	interleukin 1 beta
5.148	Izumo4	IZUMO family member 4	15.231	Mmp9	matrix metallopeptidase 9
5.167	Prkch	protein kinase C eta	15.632	LOC110350305	uncharacterized LOC110350305
5.183	Tfec	transcription factor EC	18.900	Tac1	tachykinin precursor 1
5.186	LOC110350035	uncharacterized LOC110350035	40.882	Mmp3	matrix metallopeptidase 3
5.210	LOC101711824	intersectin-2 pseudogene	55.712	Rflna	refilin A
5.210	LOC110349417	uncharacterized LOC110349417			

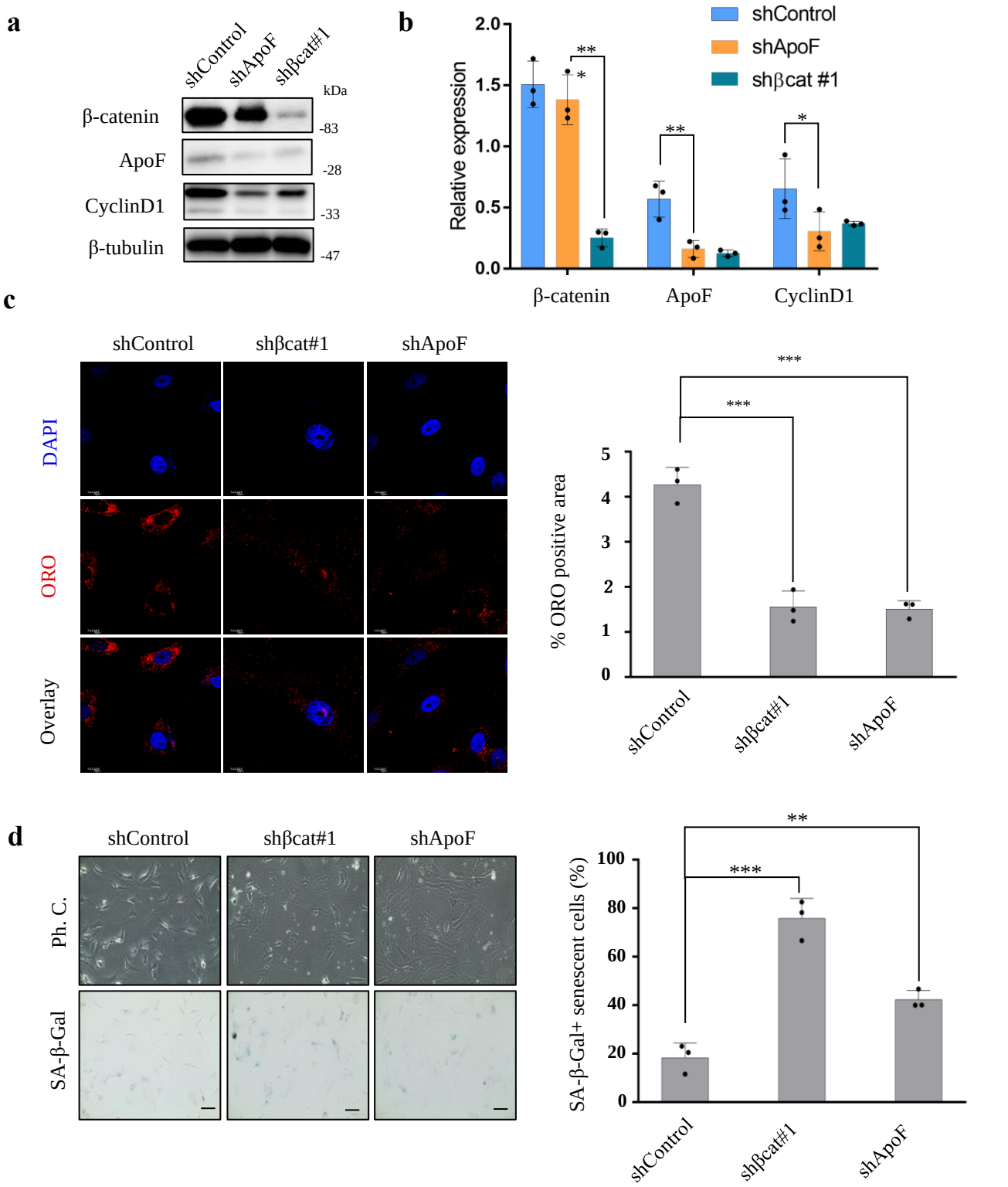

Figure 15. Knockdown of *ApoF* or *β-catenin* has similar effects in NSFs. (a) Immunoblot confirming downregulation of ApoF upon *ApoF* and *β-catenin* knockdown in NSFs. β-tubulin was used as a loading control. (**b**) Densitometric quantification of β-catenin and ApoF expression from the immunoblots shown in (a). Data are expressed as the mean ± standard deviation (n=3 culture wells/group). *P<0.05 and ***P<0.001, two-sided Student's paired *t*-test. (**c**) Immunofluorescence images demonstrating decreased abundance of lipid droplets upon *β-catenin* or *ApoF* knockdown (left). Scale bars, 10 µm. Quantitative results showing percentage coverage of cells stained with ORO versus that by total cells in the ORO assay (right). Data are expressed as the mean ± standard deviation (n=3 culture wells/group). ***P<0.001, two-sided Student's *t*-test. (**d**) Representative images showing SA-β-gal activity in control, *β-catenin*, and *ApoF* knockdown NSFs (left). Quantitative analysis of SA-β-Gal-stained cells in control, *β-catenin*, and *ApoF* knockdown cells (right). Data are expressed as the mean ± standard deviation (n=3 culture wells/group); n.s., non-significant; ** P<0.01 and *** P<0.001, two-sided Student's paired *t*-test.

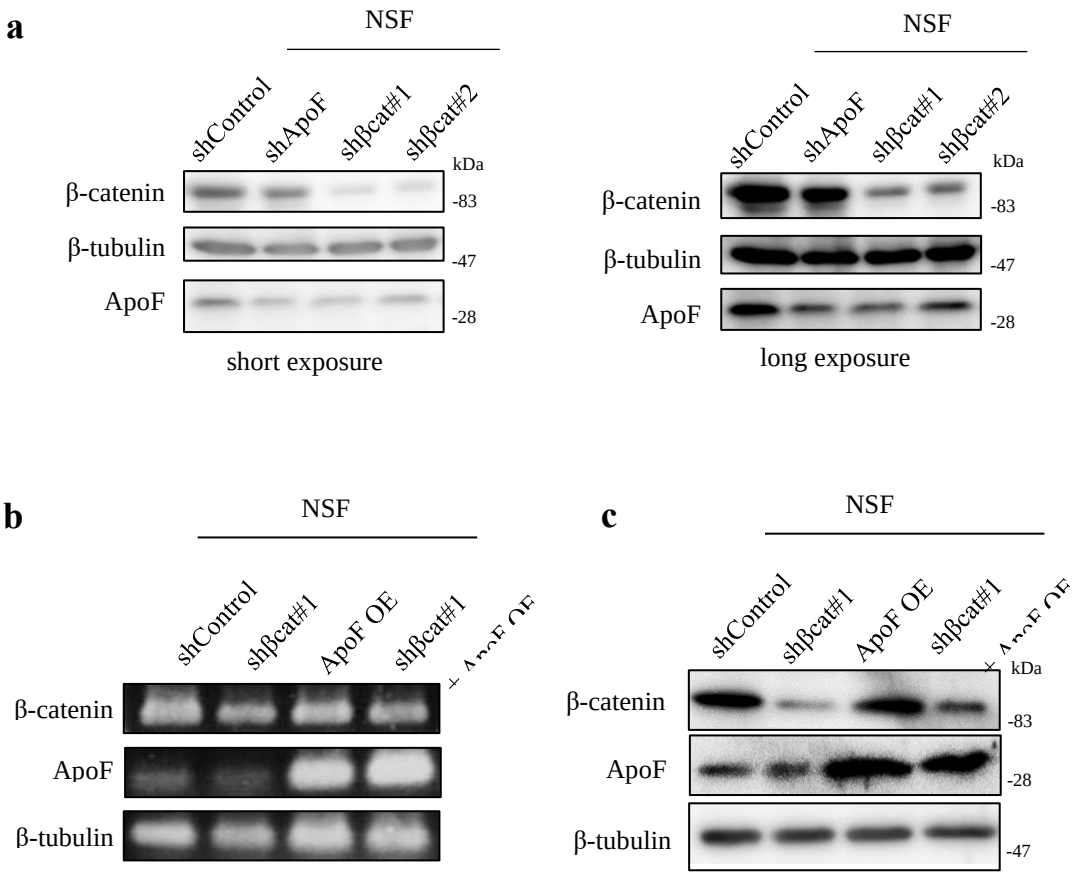

Figure 16. ApoF expression is regulated by β-catenin abundance in NSFs. (a) Immunoblot verifying ApoF downregulation upon *β-catenin* or *ApoF* knockdown. **(b)** RT-PCR quantifying expression of *β-catenin* and *ApoF*. (c) Immunoblot showing expression of β-catenin and ApoF upon *β-catenin* knockdown and/or *ApoF* overexpression.

3.6 ApoF overexpression restored the formation of lipid droplets and prevented senescence-like phenotypes induced by β-catenin knockdown

To further elucidate the function of ApoF, we overexpressed ApoF in control and β-catenin knockdown NSFs (**Fig. 16b, c**). Remarkably, ApoF overexpression restored the formation of ORO-positive lipid droplets in β-catenin knockdown NSFs, supporting that ApoF was crucial for the accumulation of lipid droplets (**Fig. 17a**). Moreover, ApoF overexpression prior to β-catenin knockdown prevented the β-catenin

knockdown-induced expansion of cell area and activation of SA-β-gal (**Fig. 17b**). Notably, ApoF overexpression after β-catenin knockdown did not restore cell area or prevent SA-β-gal activation in NSFs (**Fig. 17b, c**), consistent with the earlier observation that reloading cholesterol in senescent-like cells failed to suppress induction of SA-β-gal (**Fig. 12**). Furthermore, fluorescence analysis with BODIPY revealed that cholesterol accumulation in ORO-positive lipid was also dependent on the β-catenin-ApoE axis (**Fig. 18).** These findings suggest that ApoF is required for β-catenin-induced formation of cholesterol-enriched lipid droplets, which could be involved in the protection of NMR cells from senescence-like phenotypic changes. However, treatment of PNU-74654, an inhibitor that hinders the interaction between β-catenin and TCF-4,, in a dose-dependent manner on NSF rendered the expression of ApoF unchanged **(Figure 19)**, indicating that ApoF expression is TCF-independent.

3.7 The β-catenin-ApoF axis protected NSFs from oxidative stress

As mentioned earlier, we found that β-catenin knockdown promoted the formation of 8-OHdG, a marker for oxidative stress, suggesting that cellular senescence regulated by the β-catenin-ApoF axis is linked to oxidative stress (**Fig. 4g and Fig. 5c)**. To verify this possibility, we examined the effects of β-catenin or ApoF knockdown on the levels of reactive oxygen species (ROS) using CellROX Green Reagent, based on the previous observation that cellular senescence resulted from the accumulation of oxidative damage inflicted by ROS [83] Evidently, β-catenin and ApoF knockdown induced elevation of ROS at high intensity compared to the control (**Fig. 20a)**. Next, we used the Alamar Blue Assay to measure the cellular reducing power of NSFs as an index of cell viability. The results showed that the cell viability was significantly decreased in both β-catenin and ApoF knockdown NSFs (**Fig. 20b)**. However, treatment of N-acetyl-L-cysteine (NAC), a strong antioxidant [84], on β-catenin and ApoF knockdown NSFs restored and increased the cell viability. These findings suggest that the β-catenin-ApoF axis functions protect NMR cells from oxidative stress leading to cellular senescence associated with β-catenin/ApoF-mediated upregulation of cholesterol metabolism.

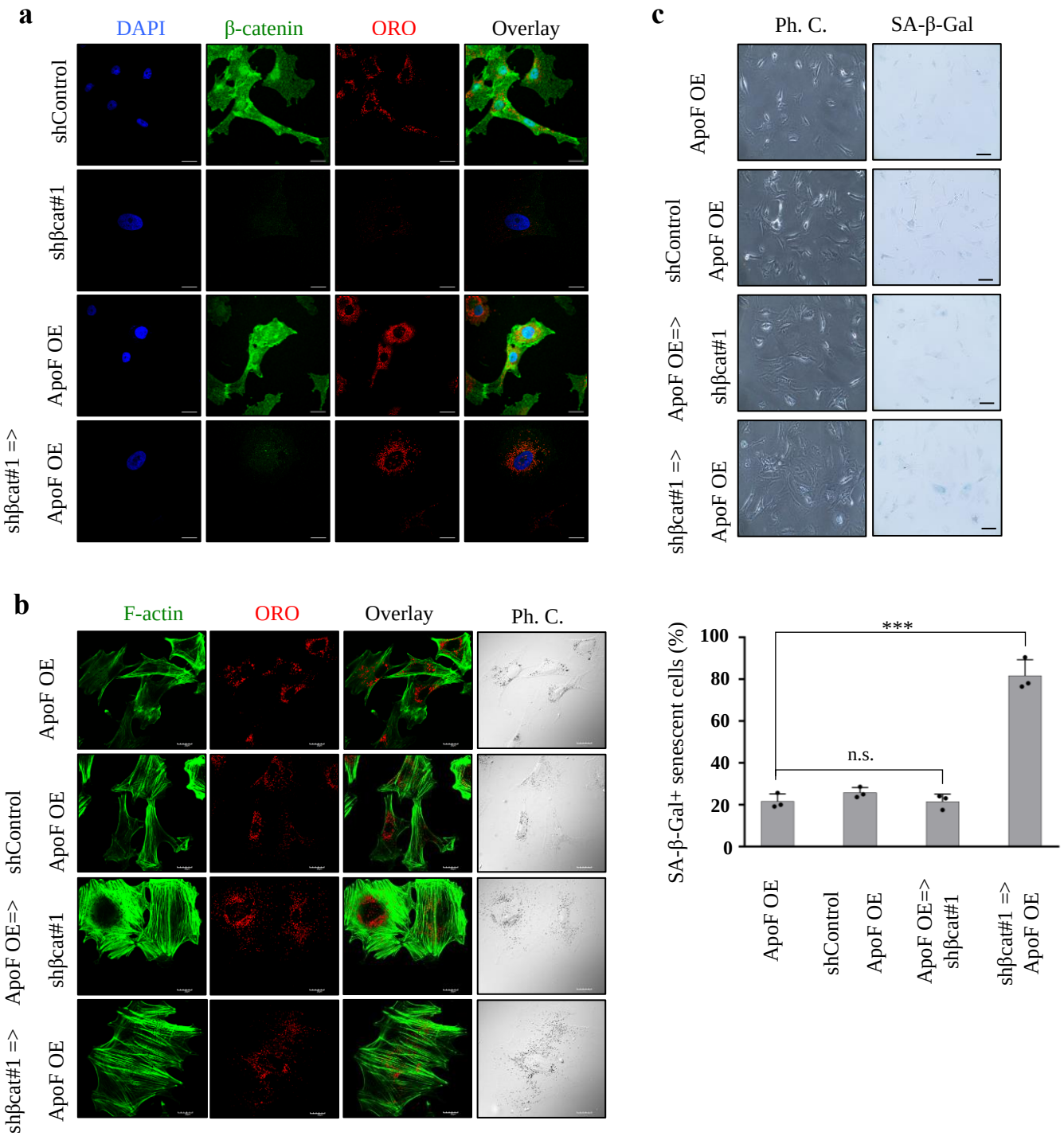

Figure 17. ApoF restores lipid droplets under conditions of β-catenin depletion. (a) Immunofluorescence images demonstrating lipid droplet restoration by *ApoF* overexpression. Scale bars, 20 μm. **(b)** Immunofluorescence images demonstrating changes in cell size and actin rearrangement upon *β-catenin* knockdown and/or *ApoF* overexpression. Scale bars, 20 μm. (**c**) SA-β-gal assay of NSFs expressing the indicated shRNA and/or ApoF cDNA (left). Scale bars, 100 μm. Quantitative results showing the percentage coverage of senescent cells versus that by total cells in the SA-β-gal assay (right). Data are expressed as the mean ± standard deviation (n=3 biological replicates). ***P<0.001 and n.s., not significant; two-sided Student's *t*-test.

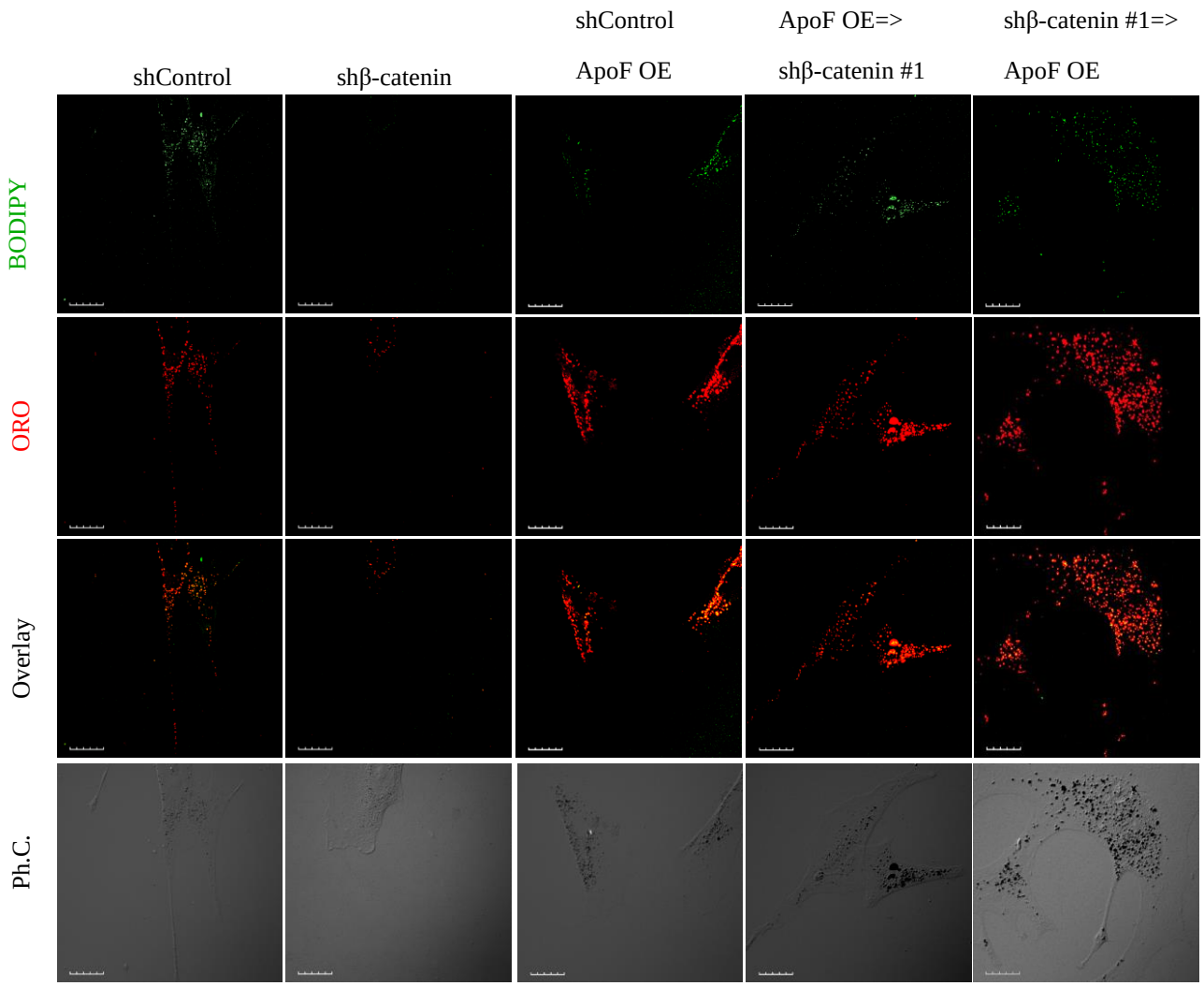

Figure 18. Overexpression of ApoF restores formation of cholesterol-enriched lipid droplets, which were suppressed by β-catenin knockdown. Immunofluorescence images demonstrating changes in formation of BODIPY- and ORO-positive lipid droplets upon β-catenin knockdown and/or ApoF overexpression. Scale bars, 20 μm.

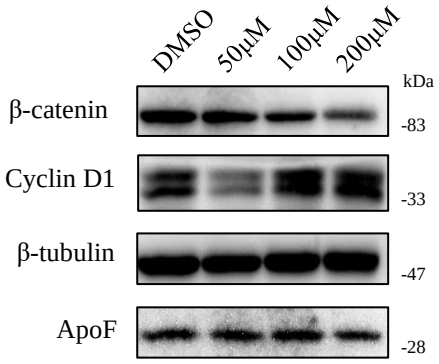

Figure 19. ApoF expression is TCF-independent. Immunoblot showing β-catenin expression levels upon treatment with increasing doses of Wnt/β-catenin antagonist PNU-74654.

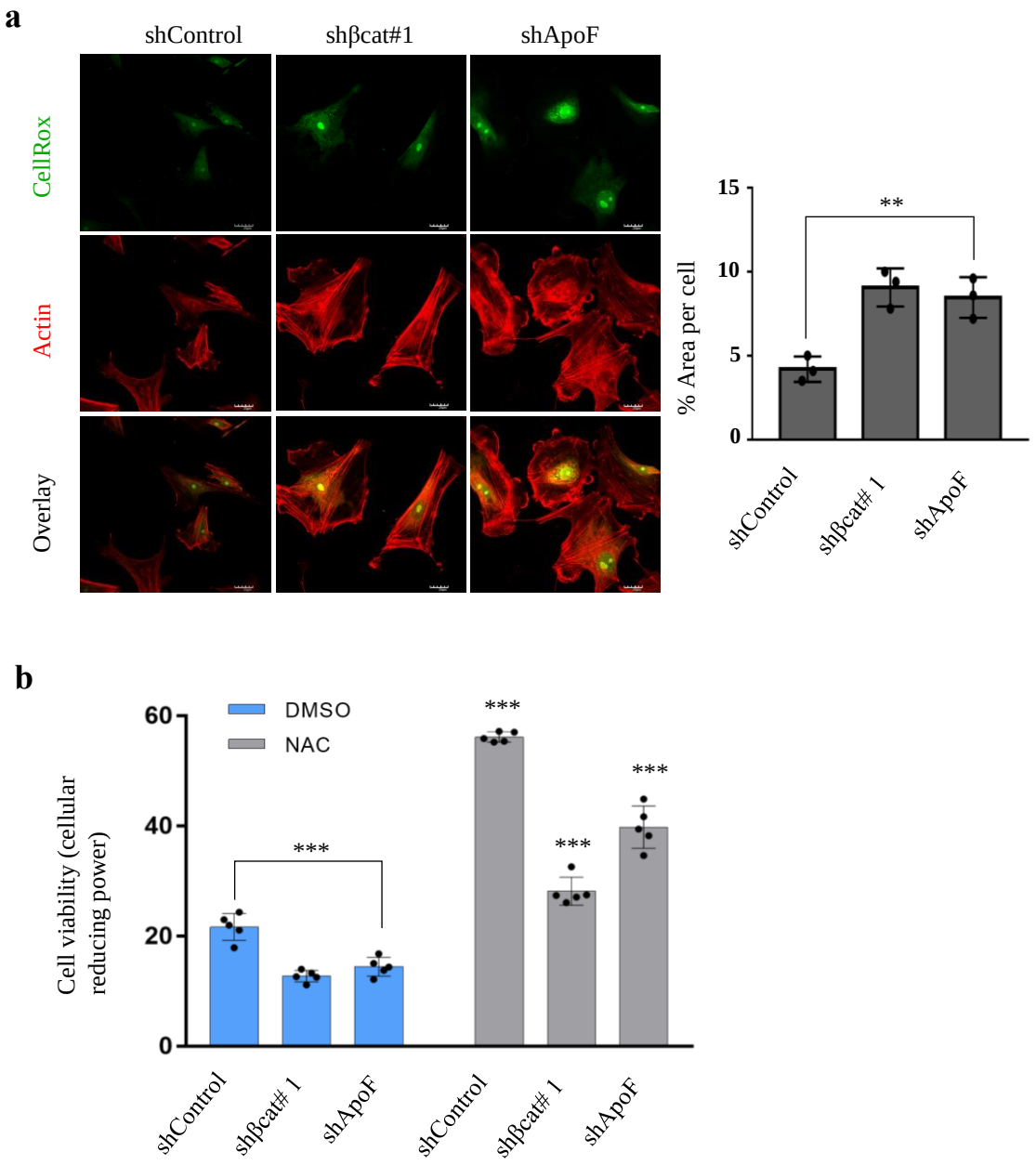

Figure 20. Induction of oxidative stress and decreased cell viability under *β-catenin* and *ApoF* knockdown conditions. (a) Immunofluorescence images showing elevated oxidative stress detected by CellRox upon *β-catenin* or *ApoF* knockdown. Scale bars, 20 μm. (left) Quantitative analysis of the CellRox in control, *β-catenin*, and *ApoF* knockdown NSFs (right). Data are expressed as the mean ± standard deviation (n=3 culture wells/group) (lower graph); **P<0.01, Student's unpaired *t*-test. **(b)** Alamar Blue assay showing decreased viability of NSFs upon *β-catenin* or *ApoF* knockdown, which was restored by treatment with NAC. Data are expressed as the mean ± standard deviation (n=5 culture wells/group). ***P<0.001, Student's unpaired *t*-test.

3.8 Overexpression of β-catenin in MSF render the ApoF expression and lipid droplets abundance level unchanged

To investigate whether the interconnection between β-catenin and lipid droplets abundance could be manifested in mouse, we overexpressed β-catenin in MSF and NIH3T3. However, the ApoF expression level remained unchanged (**Figures 21a**), and there is no dramatic accumulation of lipid droplets in both MSF and NIH3T3 cells (**Figures 21b**), suggesting that the β-catenin governed cholesterol metabolism via ApoF is uniquely established in NMR cells. As β-catenin is an oncogenic factor, one would think that NSF would grow anchorage-independently; on the contrary, the clonogenic assay shows that there are significantly fewer colonies of NSF cells form in the soft agar compared to that of the mouse. While mouse cell lines with ectopic expression of β-catenin form many and large colonies in soft agar (**Figures 22**). These findings speculate that β-catenin might have moonlighting roles in NMR.

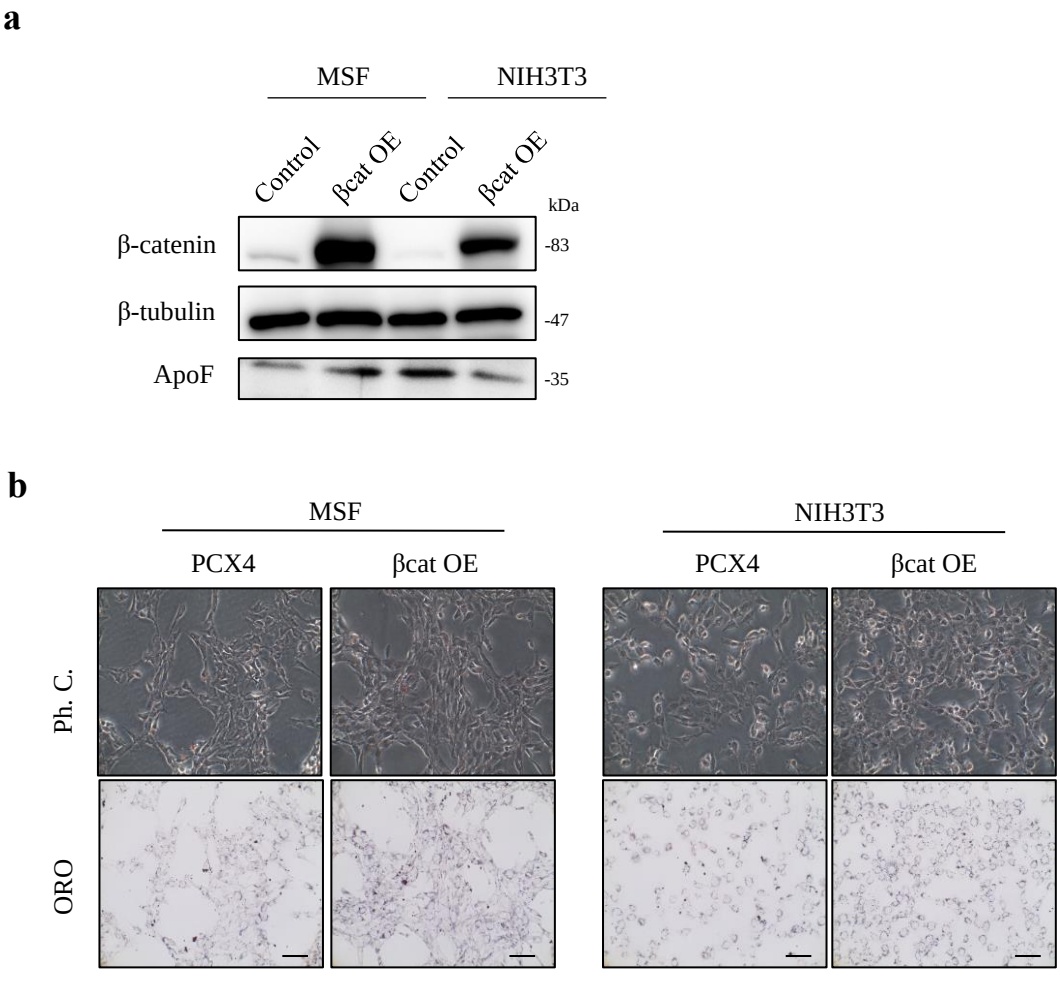

Figure 21. Overexpression of β-catenin in MSFs does not alter ApoF expression or lipid droplet abundance. (a) Immunoblot showing expression of β-catenin and ApoF in mouse cell lines after ectopic expression of *β-catenin*. **(b)** Representative phase-contrast and bright-field images of ORO-stained lipid droplets in control and *β-catenin*-overexpressing mouse cell lines. Scale bars, 100 μm.

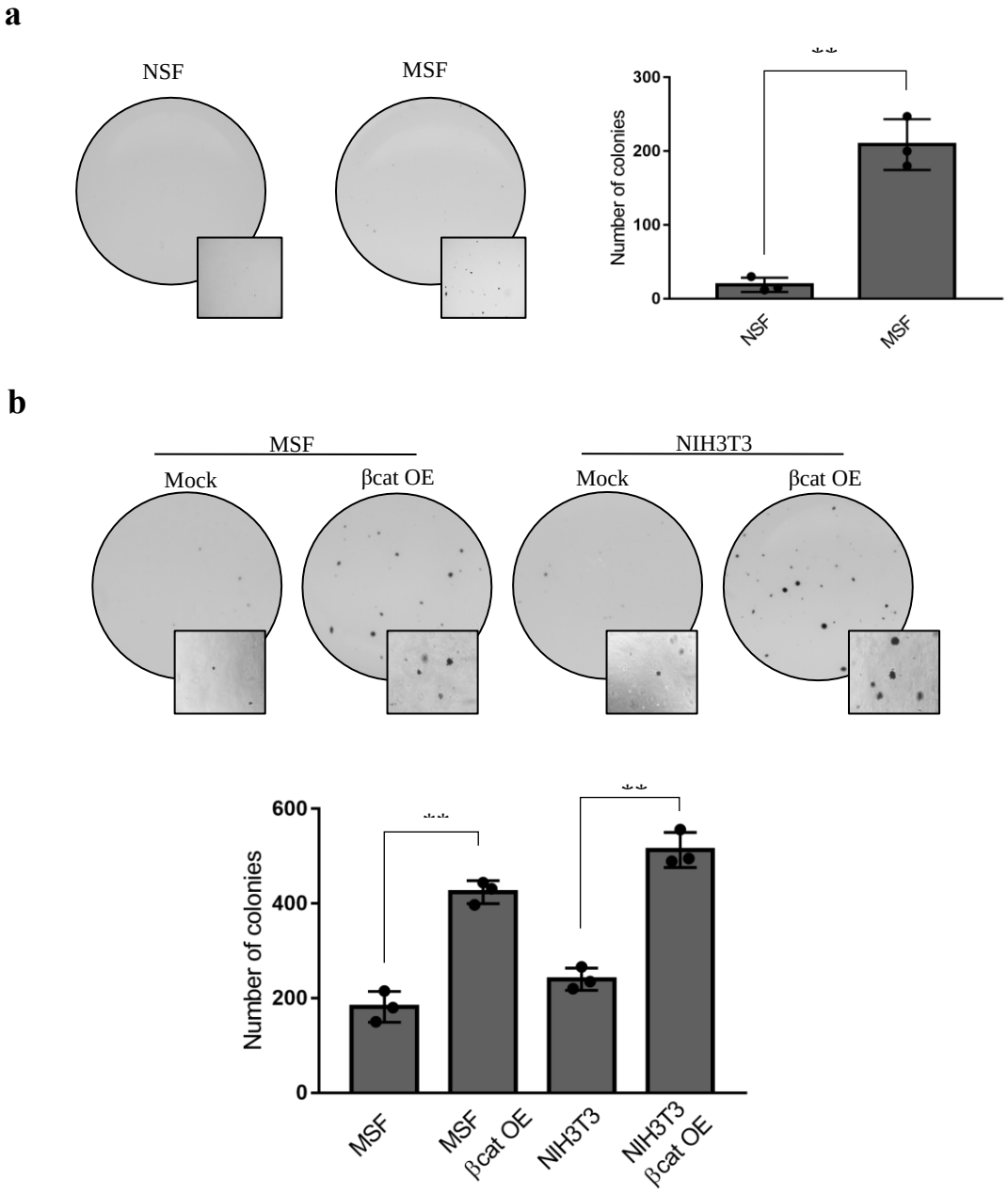

Figure 22. Differential role of β-catenin in NMR and mouse cells. (a) Soft agar colony formation assay of NSFs and MSFs. Representative dishes and enlarged views are shown (left panels). **(b)** Soft agar colony formation assay for MSFs and NIH3T3 cells with or without overexpression of *β-catenin*. Representative dishes and enlarged views are shown (upper panels). Data are expressed as the mean ± standard deviation (n=3 culture wells/group). ***p<0.001, Student's unpaired *t*-test.

CHAPTER IV

DISCUSSION

4.1 Significance of this Research

Mutation and overexpression of β-catenin are associated with increased proliferation in many cancers. However, NMR exhibits an exceptional characteristic in which accumulation of β-catenin is regulated by significantly low expression level of Axin1 in the cytoplasm, yet with no increased proliferation observed in wild-type NMR. This gives the notion that excessive β-catenin may be the working principle that drive this bizarre protective process from senescence.

The results in the Chapter III raise interesting questions regarding the functional significance of β-catenin and whether there is a correlation with longevity and anti-aging mechanism. However, further studies are required to pinpoint the working mechanism of high β-catenin level govern the cholesterol metabolism via activation of ApoF in NMR, which may contribute to anti-senescent mechanism and preventing aging. Besides that, the experimental results in this study could give a fundamental insight into how NMR achieve enhanced lifespan via β-catenin-ApoF axis. Thus, increased insights into the molecular mechanism underlying Wnt/β-catenin signalling at the interface of aging could making an advanced progress in improving human health.

4.2 Objectives achieved in this work

In normal mammalian cells, the activation of Wnt/β-catenin signaling generally plays crucial roles in cell cycle progression by upregulating mitogenic genes, such as c-Myc and Cyclin D1 [85]. Furthermore, aberrant upregulation of the Wnt/β-catenin

pathway is a major cause of colorectal cancer [86,87], which is mainly attributed to mutations in APC, Axin1, APC, or β-catenin [88,89]. Paradoxically, NMR cells expressed high levels of β-catenin and low levels of Axin1 yet target proteins such as cyclin D1 and c-Myc were expressed at considerably lower levels, potentially accounting for the slower growth rate of NMR cells. To obtain a more definitive evidence regarding the amount of cytoplasmic and nuclear β-catenin, NSF and NLF were compared and the results were confirmed to be similar in immunoblotting and immunofluorescence, with compelling results from DLR assay showing β-catenin transcriptional activity was increased in NMR cells (**Figure 1c**). Furthermore, the results from immunofluorescence has corroborated that substantial amount of β-catenin is localized in both cytoplasm and nucleus in NMR cells (**Figure 1b**). Thus, these results perchance signify the uncommon roles of β-catenin in distinctive features of NMR – enhanced longevity.

Because Axin1 scaffolds the destruction complex to promote β-catenin degradation, I postulated that Axin1 upregulation would decrease the free β-catenin pool in NMR. Furthermore, inhibition of Wnt production or overexpression of Axin1 did not affect the accumulation of β-catenin in NMR cells (**Figure 3b,c**). These unexpected observations suggested that β-catenin might play unique roles independently of the canonical Wnt/β-catenin pathway in NMRs. The negative data shown by Axin1 regulation could also be inferred from the highly phosphorylated and inactive GSK3β (**Figure 1a**), which its active form is responsible for β-catenin phosphorylation to be targeted for degradation [90]. Since meddling with the master protein GSK3β would disrupt most of the metabolic processes in the cell, I proceeded with β-catenin downregulation to examine its role in NSF. Western blot, fluorescence microscopy and DLR assay were used to validate efficient knockdown of β-catenin (**Figure 4**). Overall, these experiments confirmed the reduced expression of β-catenin at protein level and validated the experimental model. In detail, reduced expression of β-catenin by shRNA altered cellular morphology with a considerable expansion of cell area. Because free cytoplasmic β-catenin is mainly involved in cell proliferation, shβ-catenin knockdown in NSF cell lead to remarkable decrease in growth rate and β-catenin activity as shown in **Figure 4e**, f. Functionally, results of my in vitro experiments reflect clearly the transcriptional factor and key modulator of Wnt/β-catenin signalling pathway with a prominent role as regulator of cellular metabolism.

To demonstrate that β-catenin is potentially involve in tumorigenesis, I conducted soft-agar colony formation assay (clonogenic assay) in NSF and MSF cell lines, and the results from **Figure 22** revealed that MSF control group is substantially more anchorage-independent and transformed than the NSF, but evidently less tumorigenic than MSF with ectopic expression of β-catenin.

Since downregulation of β-catenin reveals the distinctive hallmarks of senescence – increased cell surface area and arrested growth, I next progressed my research to confirm the rest of the hallmarks of senescence, as β-catenin is also involved in regulating the expression of $p16^{INK4A}$ in a cell context dependent manner [91,92]. Strikingly, significant amount of shβcat NSF cells that were discernibly stained with X-gal was observed in the senescence-associated β-galactosidase assay (**Figure 7b**). Although p21 instead of p16 was used as senescence marker in this experiment, but the relative increased expression of p21 correspondingly supported that β-catenin signalling is central to cell senescence induced by cell stress such as β-catenin downregulation. This result is consistent with the study conducted by Ye et al 2007, which highlighted that Wnt/βcatenin pathway is involved in senescence regulation, as repression of Wnt2 induced senescence in stressed primary human fibroblast WI38. Furthermore, a switch from conical to non-canonical pathway in old mice resulted in senescence of hematopoietic stem cells [93].

Apart from above-mentioned results, there are several interesting findings regarding the Wnt/β-catenin pathway in NMR. For instance, to identify whether there are existential differences in Wnt canonical pathway between NMR and mouse, immunofluorescence study was conducted to determine the localization and expression levels of main proteins that comprise the β-catenin destruction complexes, such as Axin1, Adenomatous Polyposis Coli (APC), β-catenin and Glycogen Synthase Kinase 3β. And the results show that APC is primarily localized in the nucleus (**Figure 1c**), while β-catenin are distributed evenly between the nucleus and cytoplasm in NMR skin fibroblast **(Figure 1b)**. Nuclear localization of APC is also exceptional to NMR since in many cells, APC appears to be mainly cytoplasmic, with a concentration near the cell membranes [94,95]. Hence, it has been proposed that APC shuttles β-catenin from the nucleus and cytoplasm to the junctional compartment where Axin complex seems to be anchored [96]. To gain support for this, APC was revealed to contain highly conserved

nuclear export signals (NES) 3' adjacent to the mutation cluster region, enabling APC to chaperone nuclear β-catenin and reducing the latter transcriptional activity [49,97,98].

Furthermore, GSK3β has been reported to have nuclear function in downregulating the activity of β-catenin activity [99], rationalising the high β-catenin activity might be caused by hyperphosphorylation and inactivation of GSK3β in NMR (Figure 2d). While GSK3β is commonly deemed as cytoplasmic protein, several studies indicated that nuclear GSK3β is involved in mediating the nuclear/cytoplasmic distribution of several proteins including cyclin D1, GATA-4 [100], c-Myc [101], Bax [102], Snail [103] and p53 [104]. Although nuclear APC and GSk3β appear to have multiple functions, its effect on β-catenin and Wnt signalling remained unelucidated, thereby further experiments are required to grasp more insight about APC and GSK3β. Besides that, an Axin homolog, Axin 2 that is functionally similar to Axin 1 [26], was expressed and mainly localized to the nucleus in both NMR and NIH3T3 cells **(Supplementary Figure 4)**. Axin2 has been reported to induce β-catenin degradation, whereas mutants of Axin2 are dysfunctional in complex formation stabilizing β-catenin. [105]. On contrary, overexpression of Axin2 could directs β-catenin to the degradation pathway without functional APC [106], proposing that NMR could possibly utilize Axin 2 instead of Axin1 to regulate the stability of β-catenin.

In the previous context, I found that β-catenin knockdown in NSFs altered cellular morphology and function, with a considerable expansion of cell area, a remarkable decrease in growth rate, increased SA-β-Gal activity, nuclear accumulation of p21, and increased DNA damage. These phenotypes were consistent with cellular senescence, indicating that β-catenin knockdown induced cellular senescence in NSFs. On the other hand, β-catenin knockdown abolished the accumulation of cholesterol-enriched lipid droplets, and cholesterol synthesis inhibition caused senescence-like phenotypic changes similar to β-catenin knockdown. These observations suggested that abundant β-catenin in NMR cells suppressed cellular senescence via the accumulation of cholesterol in lipid droplets, consistent with a study that reported the suppressive role of cholesterol on senescence in mice [107]. I also showed that the β-catenin-ApoF axis was associated with ROS levels and cellular reducing power. In addition, cellular senescence was reported to result from the accumulation of oxidative damage inflicted by ROS of mitochondrial origin [83]. A recent study identified that mitochondrial ROS generation rates are comparable between NMRs and mice, but that the capacity to

neutralize ROS is much higher in NMRs than in mice. In conjunction with these findings, our results raise a hypothesis that the abundant cholesterol in NMR cells may serve as a ROS scavenger to suppress the onset of cellular senescence, supporting the previous study that cholesterol could function as an antioxidant to counter oxidative stress [108]. However, I could not rule out the possibility that β-catenin could also contribute to other molecular mechanisms underlying the anti-senescence effect via the upregulation of matrix metalloprotease pathway and GPCR signaling (**Fig. 14a)**.

To date, several studies have attempted to identify the functional link between Wnt/β-catenin signaling and lipid droplet formation in other contexts, but the results were somewhat contradictory. A cancer stem cell model revealed a direct correlation between Wnt pathway activity and increased lipid contents [109]. On the contrary, canonical Wnt signaling reprograms lipid metabolism by attenuating the accumulation of lipid droplets upon K-Ras overexpression [110]. In breast cancer cells, β-catenin knockdown upregulates proteins associated with lipid metabolism [111]. In the present study, however, β-catenin knockdown in NMR cells suppressed the LXR/RXR pathway involved in cholesterol metabolism and lipogenesis, indicating that the β-catenin pathway positively regulates cholesterol synthesis in NMRs. These inconsistencies between the roles of β-catenin in the regulation of lipid droplet formation further underscore the unique function of β-catenin in NMRs.

I identified ApoF, a cholesterol transfer inhibitor protein, as a unique target of β-catenin in NMR cells [112]. ApoF knockdown suppressed the accumulation of lipid droplets and promoted cellular senescence in a manner similar to β-catenin knockdown, while ApoF overexpression restored lipid droplet formation in β-catenin knockdown NSFs. These results suggest that ApoF is a crucial mediator of β-catenin-mediated accumulation of cholesterol in lipid droplets. However, the mechanisms by which ApoF expression is regulated by β-catenin are yet to be elucidated. I attempted to identify the functional link among TCF4, β-catenin, and ApoF using PNU-74654, an inhibitor preventing interaction between β-catenin and TCF [113]. Treatment of PNU-74654 in a dose-dependent manner on NSF rendered the expression of ApoF unchanged **(Fig. 19)**, indicating that ApoF expression is TCF-independent. This suggests that a unique transcription factor(s) contributes to the β-catenin-mediated regulation of ApoF expression in NMR cells, or alternatively that ApoF expression is indirectly regulated via an unknown mechanism downstream of the β-catenin signaling.

To investigate whether the interconnection between β-catenin and lipid droplets abundance could be manifested in mouse, I overexpressed β-catenin in MSFs and NIH3T3. However, the ApoF expression level remained unchanged (**Fig. 21a**), and there was no dramatic accumulation of lipid droplets in both MSFs and NIH3T3 cells (**Fig. 21b**). In addition, we observed that NSFs had no ability of anchorage-independent growth regardless of abundant β-catenin expression as expected (**Fig. 22a**), while overexpression of β-catenin in mouse cells appreciably promoted the anchorage-independent growth (**Fig. 22b**), indicating that β-catenin is oncogenic in mouse cells but not NMR cells. These results further highlight the functional difference between NMR and mouse β-catenin, and suggest that the β-catenin-governed cholesterol metabolism via ApoF is uniquely established in NMR cells.

4.3 Summary

NMR exhibit an extraordinary Wnt/β-catenin signalling pathway. It robustly expressed β-catenin, yet the target genes such as cyclin D1 and c-myc are not upregulated in response to high β-catenin level, indicating β-catenin might have atypical roles in resisting senescent/aging process. In summary, I identified constitutive high β-catenin activity in NMR cells. The increased β-catenin activity promoted the accumulation of cholesterol-enriched lipid droplets via ApoF upregulation, which could protect NMR cells from cellular senescence. These findings confirmed that NMR cells are intrinsically susceptible to cellular senescence [114], potentially due to their low rate of basal metabolism [115], which may be beneficial for longevity and cancer resistance. Hence, the upregulation of the unique β-catenin pathway in NMR cells could counterbalance their strong senescence potential, promoting longevity and survival in harsh conditions on a whole organism level. the present study could give a fundamental insight into how NMR achieve negligible senescence via β-catenin-ApoF signalling. In addition, further analysis of the molecular mechanisms underlying the anti-senescence functions of cholesterol could reveal new approaches to treatment for aging-related conditions.

References

1 Tian, X. *et al.* INK4 locus of the tumor-resistant rodent, the naked mole rat, expresses a functional p15/p16 hybrid isoform. *Proceedings of the National Academy of Sciences* **112**, 1053-1058, doi:10.1073/pnas.1418203112 (2015).

2 Tian, X. *et al.* High-molecular-mass hyaluronan mediates the cancer resistance of the naked mole rat. *Nature* **advance online publication**, doi:10.1038/nature12234 http://www.nature.com/nature/journal/vaop/ncurrent/abs/nature12234.html#supplementary-information (2013).

3 Delaney, M. A. *et al.* Initial Case Reports of Cancer in Naked Mole-rats (Heterocephalus glaber). *Veterinary pathology* **53**, 691-696, doi:10.1177/0300985816630796 (2016).

4 Edrey, Y. H., Park, T. J., Kang, H., Biney, A. & Buffenstein, R. Endocrine function and neurobiology of the longest-living rodent, the naked mole-rat. *Experimental gerontology* **46**, 116-123, doi:10.1016/j.exger.2010.09.005 (2011).

5 Larson, J. & Park, T. J. Extreme hypoxia tolerance of naked mole-rat brain. *Neuroreport* **20**, 1634-1637, doi:10.1097/WNR.0b013e32833370cf (2009).

6 Park, T. J. *et al.* Fructose-driven glycolysis supports anoxia resistance in the naked mole-rat. *Science (New York, N.Y.)* **356**, 307-311, doi:10.1126/science.aab3896 (2017).

7 Yu, C. *et al.* RNA sequencing reveals differential expression of mitochondrial and oxidation reduction genes in the long-lived naked mole-rat when compared to mice. *PLoS One* **6**, e26729, doi:10.1371/journal.pone.0026729 (2011).

8 Austad, S. N. Comparative Biology of Aging. *The Journals of Gerontology Series A: Biological Sciences and Medical Sciences* **64A**, 199-201, doi:10.1093/gerona/gln060 (2009).

9 Edrey, Y. H., Hanes, M., Pinto, M., Mele, J. & Buffenstein, R. Successful aging and sustained good health in the naked mole rat: a long-lived mammalian model for biogerontology and biomedical research. *ILAR journal* **52**, 41-53 (2011).

10 Buffenstein, R. Negligible senescence in the longest living rodent, the naked mole-rat: insights from a successfully aging species. *Journal of comparative physiology. B, Biochemical, systemic, and environmental physiology* **178**, 439-445, doi:10.1007/s00360-007-0237-5 (2008).

11 Seluanov, A. *et al.* Hypersensitivity to contact inhibition provides a clue to cancer resistance of naked mole-rat. *Proceedings of the National Academy of Sciences of the United States of America* **106**, 19352-19357, doi:10.1073/pnas.0905252106 (2009).

12 Lipman, R., Galecki, A., Burke, D. T. & Miller, R. A. Genetic loci that influence cause of death in a heterogeneous mouse stock. *The journals of gerontology. Series A, Biological sciences and medical sciences* **59**, 977-983 (2004).

13 Liang, S., Mele, J., Wu, Y., Buffenstein, R. & Hornsby, P. J. Resistance to experimental tumorigenesis in cells of a long-lived mammal, the naked mole-rat (Heterocephalus glaber). *Aging cell* **9**, 626-635, doi:10.1111/j.1474-9726.2010.00588.x (2010).

14 Klaus, A. & Birchmeier, W. Wnt signalling and its impact on development and cancer. *Nature Reviews Cancer* **8**, 387, doi:10.1038/nrc2389

https://www.nature.com/articles/nrc2389#supplementary-information (2008).

15 Mosimann, C., Hausmann, G. & Basler, K. Beta-catenin hits chromatin: regulation of Wnt target gene activation. *Nat Rev Mol Cell Biol* **10**, 276-286, doi:10.1038/nrm2654 (2009).

16 Liu, C. *et al.* Control of beta-catenin phosphorylation/degradation by a dual-kinase mechanism. *Cell* **108**, 837-847 (2002).

17 Kitagawa, M. *et al.* An F-box protein, FWD1, mediates ubiquitin-dependent proteolysis of beta-catenin. *The EMBO journal* **18**, 2401-2410, doi:10.1093/emboj/18.9.2401 (1999).

18 Aberle, H., Bauer, A., Stappert, J., Kispert, A. & Kemler, R. beta-catenin is a target for the ubiquitin-proteasome pathway. *The EMBO journal* **16**, 3797-3804, doi:10.1093/emboj/16.13.3797 (1997).

19 Cavallo, R. A. *et al.* Drosophila Tcf and Groucho interact to repress Wingless signalling activity. *Nature* **395**, 604-608, doi:10.1038/26982 (1998).

20 Roose, J. *et al.* The Xenopus Wnt effector XTcf-3 interacts with Groucho-related transcriptional repressors. *Nature* **395**, 608-612, doi:10.1038/26989 (1998).

21 Stamos, J. L., Chu, M. L., Enos, M. D., Shah, N. & Weis, W. I. Structural basis of GSK-3 inhibition by N-terminal phosphorylation and by the Wnt receptor LRP6. *eLife* **3**, e01998, doi:10.7554/eLife.01998 (2014).

22 Tetsu, O. & McCormick, F. Beta-catenin regulates expression of cyclin D1 in colon carcinoma cells. *Nature* **398**, 422-426, doi:10.1038/18884 (1999).

23 He, T. C. *et al.* Identification of c-MYC as a target of the APC pathway. *Science (New York, N.Y.)* **281**, 1509-1512 (1998).

24 Batlle, E. *et al.* Beta-catenin and TCF mediate cell positioning in the intestinal epithelium by controlling the expression of EphB/ephrinB. *Cell* **111**, 251-263 (2002).

25 Goentoro, L. & Kirschner, M. W. Evidence that fold-change, and not absolute level, of beta-catenin dictates Wnt signaling. *Molecular cell* **36**, 872-884, doi:10.1016/j.molcel.2009.11.017 (2009).

26 Lustig, B. *et al.* Negative feedback loop of Wnt signaling through upregulation of conductin/axin2 in colorectal and liver tumors. *Molecular and cellular biology* **22**, 1184-1193 (2002).

27 Yan, D. *et al.* Elevated expression of axin2 and hnkd mRNA provides evidence that Wnt/beta -catenin signaling is activated in human colon tumors. *Proceedings of the National Academy of Sciences of the United States of America* **98**, 14973-14978, doi:10.1073/pnas.261574498 (2001).

28 Jho, E. H. *et al.* Wnt/beta-catenin/Tcf signaling induces the transcription of Axin2, a negative regulator of the signaling pathway. *Molecular and cellular biology* **22**, 1172-1183 (2002).

29 Hedgepeth, C. M., Deardorff, M. A. & Klein, P. S. Xenopus axin interacts with glycogen synthase kinase-3 beta and is expressed in the anterior midbrain. *Mechanisms of Development* **80**, 147-151, doi:https://doi.org/10.1016/S0925-4773(98)00203-2 (1999).

30 Ikeda, S. *et al.* Axin, a negative regulator of the Wnt signaling pathway, forms a complex with GSK-3beta and beta-catenin and promotes GSK-3beta-dependent phosphorylation of beta-catenin. *The EMBO journal* **17**, 1371-1384, doi:10.1093/emboj/17.5.1371 (1998).

31 Hart, M. J., de los Santos, R., Albert, I. N., Rubinfeld, B. & Polakis, P. Downregulation of beta-catenin by human Axin and its association with the APC tumor suppressor, beta-catenin and GSK3 beta. *Current biology : CB* **8**, 573-581 (1998).

32 Li, V. S. *et al.* Wnt signaling through inhibition of beta-catenin degradation in an intact Axin1 complex. *Cell* **149**, 1245-1256, doi:10.1016/j.cell.2012.05.002 (2012).

33 Bilic, J. *et al.* Wnt induces LRP6 signalosomes and promotes dishevelled-dependent LRP6 phosphorylation. *Science (New York, N.Y.)* **316**, 1619-1622, doi:10.1126/science.1137065 (2007).

34 Kim, S. & Jho, E. H. The protein stability of Axin, a negative regulator of Wnt signaling, is regulated by Smad ubiquitination regulatory factor 2 (Smurf2). *The Journal of biological chemistry* **285**, 36420-36426, doi:10.1074/jbc.M110.137471 (2010).

35 Schwarz-Romond, T. *et al.* The DIX domain of Dishevelled confers Wnt signaling by dynamic polymerization. *Nature structural & molecular biology* **14**, 484-492, doi:10.1038/nsmb1247 (2007).

36 Kim, S. E. *et al.* Wnt stabilization of beta-catenin reveals principles for morphogen receptor-scaffold assemblies. *Science (New York, N.Y.)* **340**, 867-870, doi:10.1126/science.1232389 (2013).

37 Anvarian, Z. *et al.* Axin cancer mutants form nanoaggregates to rewire the Wnt signaling network. *Nature structural & molecular biology* **23**, 324-332, doi:10.1038/nsmb.3191 (2016).

38 Leung, J. Y. *et al.* Activation of AXIN2 expression by beta-catenin-T cell factor. A feedback repressor pathway regulating Wnt signaling. *The Journal of biological chemistry* **277**, 21657-21665, doi:10.1074/jbc.M200139200 (2002).

39 Powell, S. M. *et al.* APC mutations occur early during colorectal tumorigenesis. *Nature* **359**, 235-237, doi:10.1038/359235a0 (1992).

40 Senda, T., Iizuka-Kogo, A., Onouchi, T. & Shimomura, A. Adenomatous polyposis coli (APC) plays multiple roles in the intestinal and colorectal epithelia. *Medical molecular morphology* **40**, 68-81, doi:10.1007/s00795-006-0352-5 (2007).

41 Kohler, E. M., Chandra, S. H., Behrens, J. & Schneikert, J. Beta-catenin degradation mediated by the CID domain of APC provides a model for the selection of APC mutations in colorectal, desmoid and duodenal tumours. *Human molecular genetics* **18**, 213-226, doi:10.1093/hmg/ddn338 (2009).

42 Roberts, D. M. *et al.* Deconstructing the sscatenin destruction complex: mechanistic roles for the tumor suppressor APC in regulating Wnt signaling. *Molecular biology of the cell* **22**, 1845-1863, doi:10.1091/mbc.E10-11-0871 (2011).

43 Choi, S. H., Estaras, C., Moresco, J. J., Yates, J. R., 3rd & Jones, K. A. alpha-Catenin interacts with APC to regulate beta-catenin proteolysis and transcriptional repression of Wnt target genes. *Genes & development* **27**, 2473-2488, doi:10.1101/gad.229062.113 (2013).

44 Rubinfeld, B. *et al.* Stabilization of beta-catenin by genetic defects in melanoma cell lines. *Science (New York, N.Y.)* **275**, 1790-1792 (1997).

45 Rubinfeld, B. *et al.* Binding of GSK3beta to the APC-beta-catenin complex and regulation of complex assembly. *Science (New York, N.Y.)* **272**, 1023-1026 (1996).

46 Munemitsu, S., Albert, I., Souza, B., Rubinfeld, B. & Polakis, P. Regulation of intracellular beta-catenin levels by the adenomatous polyposis coli (APC) tumor-suppressor protein. *Proceedings of the National Academy of Sciences of the United States of America* **92**, 3046-3050 (1995).

47 Neufeld, K. L. & White, R. L. Nuclear and cytoplasmic localizations of the adenomatous polyposis coli protein. *Proceedings of the National Academy of Sciences of the United States of America* **94**, 3034-3039 (1997).

48 Huelsken, J., Vogel, R., Erdmann, B., Cotsarelis, G. & Birchmeier, W. beta-Catenin controls hair follicle morphogenesis and stem cell differentiation in the skin. *Cell* **105**, 533-545 (2001).

49 Rosin-Arbesfeld, R., Cliffe, A., Brabletz, T. & Bienz, M. Nuclear export of the APC tumour suppressor controls β-catenin function in transcription. *The EMBO journal* **22**, 1101-1113, doi:10.1093/emboj/cdg105 (2003).

50 Henderson, B. R. & Fagotto, F. The ins and outs of APC and β-catenin nuclear transport. *EMBO reports* **3**, 834-839, doi:10.1093/embo-reports/kvf181 (2002).

51 Dale, T. C. Signal transduction by the Wnt family of ligands. *The Biochemical journal* **329 (Pt 2)**, 209-223 (1998).

52 Dierick, H. & Bejsovec, A. Cellular mechanisms of wingless/Wnt signal transduction. *Current topics in developmental biology* **43**, 153-190 (1999).

53 Miyoshi, Y. *et al.* Frequent mutations in the beta-catenin gene in desmoid tumors from patients without familial adenomatous polyposis. *Oncology research* **10**, 591-594 (1998).

54 Sparks, A. B., Morin, P. J., Vogelstein, B. & Kinzler, K. W. Mutational analysis of the APC/beta-catenin/Tcf pathway in colorectal cancer. *Cancer research* **58**, 1130-1134 (1998).

55 Sutherland, C. What Are the bona fide GSK3 Substrates? *International journal of Alzheimer's disease* **2011**, 505607, doi:10.4061/2011/505607 (2011).

56 Uchida, Y. *et al.* Semaphorin3A signalling is mediated via sequential Cdk5 and GSK3beta phosphorylation of CRMP2: implication of common phosphorylating mechanism underlying axon guidance and Alzheimer's disease. *Genes to cells : devoted to molecular & cellular mechanisms* **10**, 165-179, doi:10.1111/j.1365-2443.2005.00827.x (2005).

57 Hagen, T. & Vidal-Puig, A. Characterisation of the phosphorylation of beta-catenin at the GSK-3 priming site Ser45. *Biochemical and biophysical research communications* **294**, 324-328, doi:10.1016/s0006-291x(02)00485-0 (2002).

58 Scales, T. M., Lin, S., Kraus, M., Goold, R. G. & Gordon-Weeks, P. R. Nonprimed and DYRK1A-primed GSK3 beta-phosphorylation sites on MAP1B regulate microtubule dynamics in growing axons. *J Cell Sci* **122**, 2424-2435, doi:10.1242/jcs.040162 (2009).

59 Zeng, X. *et al.* A dual-kinase mechanism for Wnt co-receptor phosphorylation and activation. *Nature* **438**, 873-877, doi:10.1038/nature04185 (2005).

60 Jope, R. S. & Johnson, G. V. The glamour and gloom of glycogen synthase kinase-3. *Trends Biochem Sci* **29**, 95-102, doi:10.1016/j.tibs.2003.12.004 (2004).

61 Stambolic, V. & Woodgett, J. R. Mitogen inactivation of glycogen synthase kinase-3 beta in intact cells via serine 9 phosphorylation. *Biochemical Journal* **303**, 701-704 (1994).

62 Thornton, T. M. *et al.* Phosphorylation by p38 MAPK as an alternative pathway for GSK3beta inactivation. *Science (New York, N.Y.)* **320**, 667-670, doi:10.1126/science.1156037 (2008).

63 Miyawaki, S. *et al.* Tumour resistance in induced pluripotent stem cells derived from naked mole-rats. *Nat Commun* **7**, 11471, doi:10.1038/ncomms11471 (2016).

64 Akagi, T., Sasai, K. & Hanafusa, H. Refractory nature of normal human diploid fibroblasts with respect to oncogene-mediated transformation. *Proc. Natl. Acad. Sci. U. S. A.* **100**, 13567-13572, doi:10.1073/pnas.1834876100 (2003).

65 Krämer, A., Green, J., Pollard, J., Jr. & Tugendreich, S. Causal analysis approaches in Ingenuity Pathway Analysis. *Bioinformatics (Oxford, England)* **30**, 523-530 (2013).

66 Koopman, R., Schaart, G. & Hesselink, M. K. Optimisation of oil red O staining permits combination with immunofluorescence and automated quantification of lipids. *Histochem. Cell Biol.* **116**, 63-68, doi:10.1007/s004180100297 (2001).

67 Christian, A. E., Haynes, M. P., Phillips, M. C. & Rothblat, G. H. Use of cyclodextrins for manipulating cellular cholesterol content. *J Lipid Res* **38**, 2264-2272 (1997).

68 Zidovetzki, R. & Levitan, I. Use of cyclodextrins to manipulate plasma membrane cholesterol content: Evidence, misconceptions and control strategies. *Biochimica et Biophysica Acta (BBA) - Biomembranes* **1768**, 1311-1324, doi:https://doi.org/10.1016/j.bbamem.2007.03.026 (2007).

69 Oneyama, C. *et al.* The lipid raft-anchored adaptor protein Cbp controls the oncogenic potential of c-Src. *Mol. Cell* **30**, 426-436, doi:10.1016/j.molcel.2008.03.026 (2008).

70 Huang, Y. *et al.* IWP2 impairs the development of porcine somatic cell nuclear transfer embryos via Wnt signaling pathway inactivation. *Biomed Rep* **7**, 36-40, doi:10.3892/br.2017.918 (2017).

71 Korinek, V. *et al.* Constitutive transcriptional activation by a beta-catenin-Tcf complex in APC-/- colon carcinoma. *Science* **275**, 1784-1787 (1997).

72 Kasai, H. *et al.* Formation of 8-hydroxyguanine moiety in cellular DNA by agents producing oxygen radicals and evidence for its repair. *Carcinogenesis* **7**, 1849-1851, doi:10.1093/carcin/7.11.1849 (1986).

73 Cutler, R. G. Antioxidants and aging. *Am. J. Clin. Nutr.* **53**, 373S-379S, doi:10.1093/ajcn/53.1.373S (1991).

74 Sherwood, S. W., Rush, D., Ellsworth, J. L. & Schimke, R. T. Defining cellular senescence in IMR-90 cells: a flow cytometric analysis. *Proc. Natl. Acad. Sci. U. S. A.* **85**, 9086-9090, doi:10.1073/pnas.85.23.9086 (1988).

75 Chen, H., Li, Y. & Tollefsbol, T. O. Cell senescence culturing methods. *Methods Mol. Biol.* **1048**, 1-10, doi:10.1007/978-1-62703-556-9_1 (2013).

76 Geltinger, F. *et al.* The transfer of specific mitochondrial lipids and proteins to lipid droplets contributes to proteostasis upon stress and aging in the eukaryotic model system Saccharomyces cerevisiae. *Geroscience* **42**, 19-38, doi:10.1007/s11357-019-00103-0 (2020).

77 Shimabukuro, M. K. *et al.* Lipid-laden cells differentially distributed in the aging brain are functionally active and correspond to distinct phenotypes. *Sci. Rep.* **6**, 23795, doi:10.1038/srep23795 (2016).

78 Lagor, W. R. *et al.* The effects of apolipoprotein F deficiency on high density lipoprotein cholesterol metabolism in mice. *PLoS One* **7**, e31616-e31616, doi:10.1371/journal.pone.0031616 (2012).

79 Day, J. R. *et al.* Purification and molecular cloning of human apolipoprotein F. *Biochemical and biophysical research communications* **203**, 1146-1151, doi:10.1006/bbrc.1994.2302 (1994).

80 Morton, R. E. & Steinbrunner, J. V. Determination of lipid transfer inhibitor protein activity in human lipoprotein-deficient plasma. *Arteriosclerosis and thrombosis : a journal of vascular biology* **13**, 1843-1851, doi:10.1161/01.atv.13.12.1843 (1993).

81 Wang, X., Driscoll, D. M. & Morton, R. E. Molecular cloning and expression of lipid transfer inhibitor protein reveals its identity with apolipoprotein F. *The Journal of biological chemistry* **274**, 1814-1820, doi:10.1074/jbc.274.3.1814 (1999).

82 Serdyuk, A. P. & Morton, R. E. Lipid transfer inhibitor protein defines the participation of lipoproteins in lipid transfer reactions: CETP has no preference for cholesteryl esters in HDL versus LDL. *Arteriosclerosis, thrombosis, and vascular biology* **19**, 718-726, doi:10.1161/01.atv.19.3.718 (1999).

83 Barja, G. Updating the mitochondrial free radical theory of aging: an integrated view, key aspects, and confounding concepts. *Antioxid Redox Signal* **19**, 1420-1445, doi:10.1089/ars.2012.5148 (2013).

84 Maheshwari, A., Misro, M. M., Aggarwal, A., Sharma, R. K. & Nandan, D. N-acetyl-L-cysteine counteracts oxidative stress and prevents H2O2 induced germ cell apoptosis through down-regulation of caspase-9 and JNK/c-Jun. *Molecular reproduction and development* **78**, 69-79, doi:10.1002/mrd.21268 (2011).

85 Herbst, A. *et al.* Comprehensive analysis of beta-catenin target genes in colorectal carcinoma cell lines with deregulated Wnt/beta-catenin signaling. *BMC genomics* **15**, 74, doi:10.1186/1471-2164-15-74 (2014).

86 White, B. D., Chien, A. J. & Dawson, D. W. Dysregulation of Wnt/β-catenin Signaling in Gastrointestinal Cancers. *Gastroenterology* **142**, 219-232, doi:10.1053/j.gastro.2011.12.001 (2012).

87 Brabletz, T. *et al.* Variable beta-catenin expression in colorectal cancers indicates tumor progression driven by the tumor environment. *Proceedings of the National Academy of Sciences of the United States of America* **98**, 10356-10361, doi:10.1073/pnas.171610498 (2001).

88 Salahshor, S. & Woodgett, J. R. The links between axin and carcinogenesis. *Journal of clinical pathology* **58**, 225-236, doi:10.1136/jcp.2003.009506 (2005).

89 Kinzler, K. W. & Vogelstein, B. Lessons from hereditary colorectal cancer. *Cell* **87**, 159-170 (1996).

90 Wu, D. & Pan, W. GSK3: a multifaceted kinase in Wnt signaling. *Trends in biochemical sciences* **35**, 161-168, doi:10.1016/j.tibs.2009.10.002 (2010).

91 Delmas, V. *et al.* Beta-catenin induces immortalization of melanocytes by suppressing p16INK4a expression and cooperates with N-Ras in melanoma development. *Genes & development* **21**, 2923-2935, doi:10.1101/gad.450107 (2007).

92 Bishop, C. L. *et al.* Primary cilium-dependent and -independent Hedgehog signaling inhibits p16(INK4A). *Molecular cell* **40**, 533-547, doi:10.1016/j.molcel.2010.10.027 (2010).

93 Florian, M. C. *et al.* A canonical to non-canonical Wnt signalling switch in haematopoietic stem-cell ageing. *Nature* **503**, 392-396, doi:10.1038/nature12631 (2013).

94 Zhang, F., White, R. L. & Neufeld, K. L. Phosphorylation near nuclear localization signal regulates nuclear import of adenomatous polyposis coli protein. *Proceedings of the National Academy of Sciences* **97**, 12577-12582, doi:10.1073/pnas.230435597 (2000).

95 Nathke, I. S., Adams, C. L., Polakis, P., Sellin, J. H. & Nelson, W. J. The adenomatous polyposis coli tumor suppressor protein localizes to plasma membrane sites involved in active cell migration. *J Cell Biol* **134**, 165-179 (1996).

96 Bienz, M. APC: the plot thickens. *Current opinion in genetics & development* **9**, 595-603 (1999).

97 Henderson, B. R. Nuclear-cytoplasmic shuttling of APC regulates beta-catenin subcellular localization and turnover. *Nature cell biology* **2**, 653-660, doi:10.1038/35023605 (2000).

98 Rosin-Arbesfeld, R., Townsley, F. & Bienz, M. The APC tumour suppressor has a nuclear export function. *Nature* **406**, 1009-1012, doi:10.1038/35023016 (2000).

99 Caspi, M., Zilberberg, A., Eldar-Finkelman, H. & Rosin-Arbesfeld, R. Nuclear GSK-3beta inhibits the canonical Wnt signalling pathway in a beta-catenin phosphorylation-independent manner. *Oncogene* **27**, 3546-3555, doi:10.1038/sj.onc.1211026 (2008).

100 Morisco, C. *et al.* Glycogen synthase kinase 3beta regulates GATA4 in cardiac myocytes. *The Journal of biological chemistry* **276**, 28586-28597, doi:10.1074/jbc.M103166200 (2001).

101 Gregory, M. A., Qi, Y. & Hann, S. R. Phosphorylation by glycogen synthase kinase-3 controls c-myc proteolysis and subnuclear localization. *The Journal of biological chemistry* **278**, 51606-51612, doi:10.1074/jbc.M310722200 (2003).

102 Linseman, D. A. *et al.* Glycogen synthase kinase-3beta phosphorylates Bax and promotes its mitochondrial localization during neuronal apoptosis. *The Journal of neuroscience : the official journal of the Society for Neuroscience* **24**, 9993-10002, doi:10.1523/jneurosci.2057-04.2004 (2004).

103 Yook, J. I., Li, X. Y., Ota, I., Fearon, E. R. & Weiss, S. J. Wnt-dependent regulation of the E-cadherin repressor snail. *The Journal of biological chemistry* **280**, 11740-11748, doi:10.1074/jbc.M413878200 (2005).

104 Watcharasit, P. *et al.* Direct, activating interaction between glycogen synthase kinase-3beta and p53 after DNA damage. *Proceedings of the National Academy of Sciences of the United States of America* **99**, 7951-7955, doi:10.1073/pnas.122062299 (2002).

105 Hulsken, J., Birchmeier, W. & Behrens, J. E-cadherin and APC compete for the interaction with beta-catenin and the cytoskeleton. *J Cell Biol* **127**, 2061-2069 (1994).

106 Behrens, J. *et al.* Functional interaction of an axin homolog, conductin, with beta-catenin, APC, and GSK3beta. *Science (New York, N.Y.)* **280**, 596-599 (1998).

107 Zhang, M. *et al.* Cholesterol Retards Senescence in Bone Marrow Mesenchymal Stem Cells by Modulating Autophagy and ROS/p53/p21(Cip1/Waf1) Pathway. *Oxid. Med. Cell. Longev.* **2016**, 7524308, doi:10.1155/2016/7524308 (2016).

108 Smith, L. L. Another cholesterol hypothesis: cholesterol as antioxidant. *Free Radic. Biol. Med.* **11**, 47-61, doi:10.1016/0891-5849(91)90187-8 (1991).

109 Tirinato, L. *et al.* Lipid Droplets: A New Player in Colorectal Cancer Stem Cells Unveiled by Spectroscopic Imaging. *STEM CELLS* **33**, doi:10.1002/stem.1837 (2015).

110 Yao, Y. *et al.* Canonical Wnt Signaling Remodels Lipid Metabolism in Zebrafish Hepatocytes following Ras Oncogenic Insult. *Cancer research* **78**, 5548, doi:10.1158/0008-5472.CAN-17-3964 (2018).

111 Vergara, D. *et al.* β-Catenin Knockdown Affects Mitochondrial Biogenesis and Lipid Metabolism in Breast Cancer Cells. *Frontiers in Physiology* **8**, doi:10.3389/fphys.2017.00544 (2017).

112 Morton, R. E., Liu, Y. & Izem, L. ApoF knockdown increases cholesteryl ester transfer to LDL and impairs cholesterol clearance in fat-fed hamsters. *Journal of Lipid Research* **60**, 1868-1879, doi:10.1194/jlr.RA119000171 (2019).

113 Trosset, J. Y. *et al.* Inhibition of protein-protein interactions: the discovery of druglike beta-catenin inhibitors by combining virtual and biophysical screening. *Proteins* **64**, 60-67, doi:10.1002/prot.20955 (2006).

114 Zhao, Y. *et al.* Naked mole rats can undergo developmental, oncogene-induced and DNA damage-induced cellular senescence. *Proceedings of the National Academy of Sciences of the United States of America* **115**, 1801-1806, doi:10.1073/pnas.1721160115 (2018).

115 Lewis, K. N., Rubinstein, N. D. & Buffenstein, R. A window into extreme longevity; the circulating metabolomic signature of the naked mole-rat, a mammal that shows negligible senescence. *Geroscience* **40**, 105-121, doi:10.1007/s11357-018-0014-2 (2018).

APPENDICES

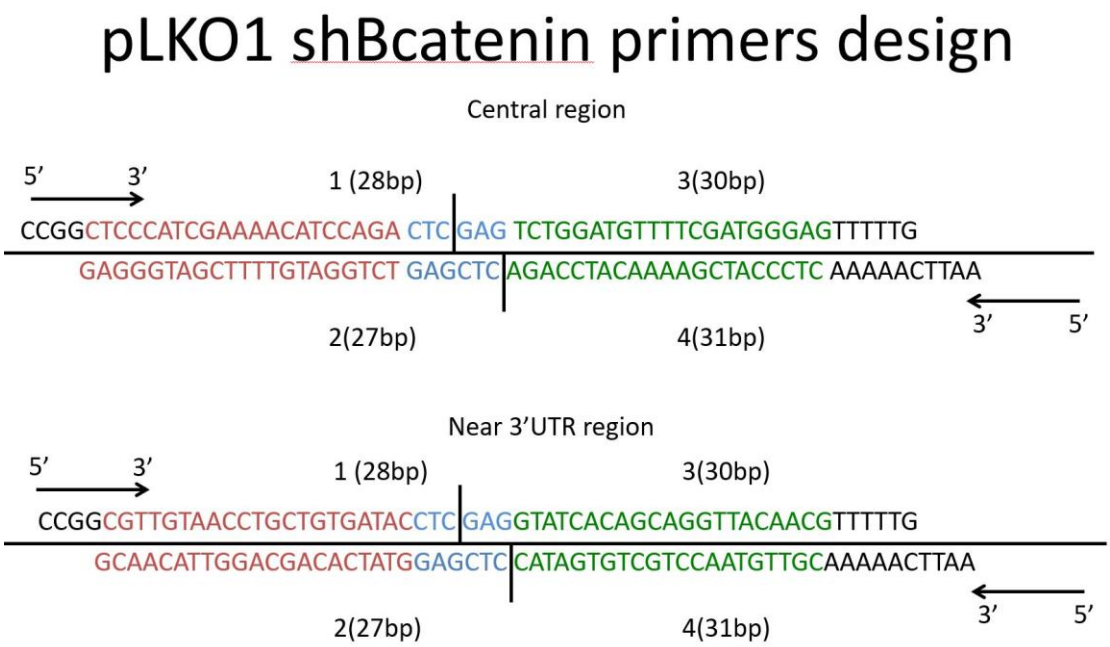

Supplementary Figure 1. Sequences for shβ-catenin targeting central and UTR region. Red: target sequence; Blue: linker sequence; Green: Complementary target sequence; Black: Restriction site.

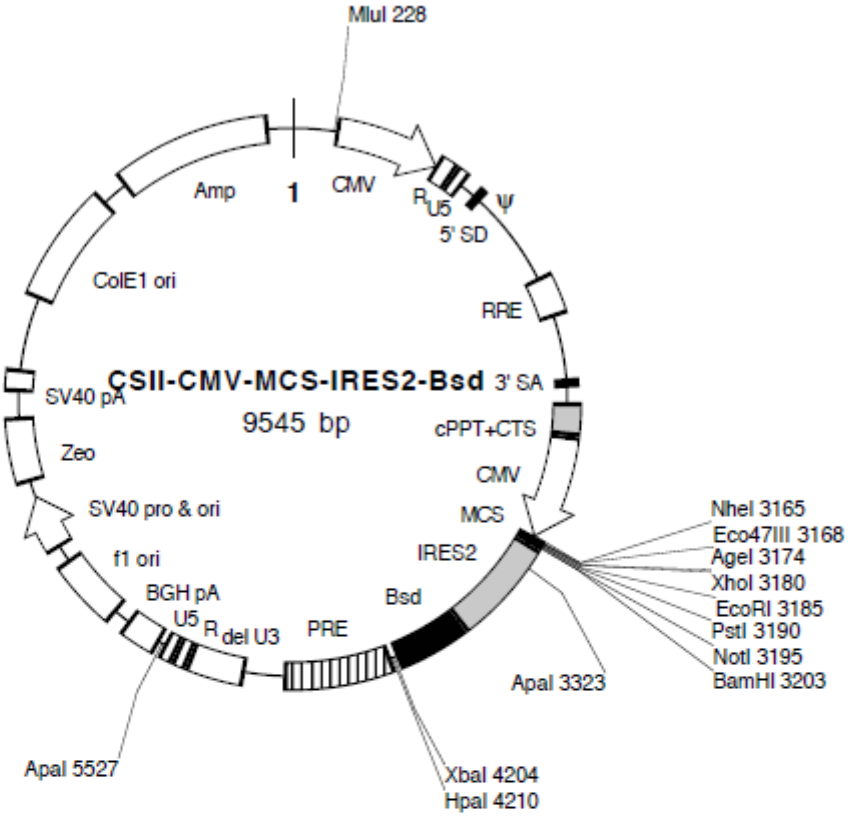

Plasmid name: CSII-CMV-MCS-IRES2-Bsd
Plasmid size: 9545 bp
Note
CMV: Human cytomegalovirus immediate early promoter
ψ: Packaging signal
5'SD: 5' splicing donor site
3'SA: 3' splicing acceptor site
RRE: Rev responsive element
cPPT: Central polypurine tract
CTS: Central termination sequence
MCS: Multiple cloning site
IRES2: Encephalomyocarditis virus internal ribosomal entry site
Bsd: Blasticidin resistance gene
PRE: Woodchuck hepatitis virus posttranscriptional regulatory element
del U3: Deletion of enhancer and promoter sequences in the U3 region
BGH pA: Bovine growth hormone polyadenylation signal
SV40 pro & ori: SV40 early promoter and origin
Zeo: Zeocin resistance gene
SV40 pA: SV40 polyadenylation signal
Amp: Ampicillin resistance gene

Supplementary Figure 2. Vector map of CSII-CMV-MCS-IRES2-Bsd; used for lentiviral overexpression of Axin1 in NSF.

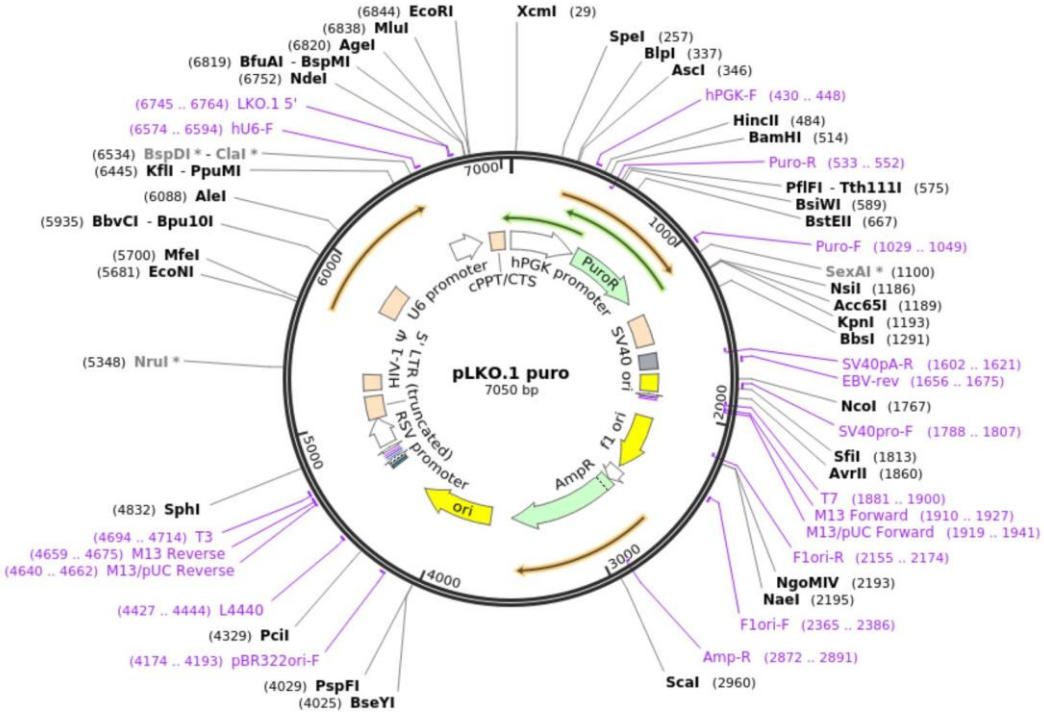

Supplementary Figure 3. Vector map of pLKO1; used for β-catenin knockdown in NSF.

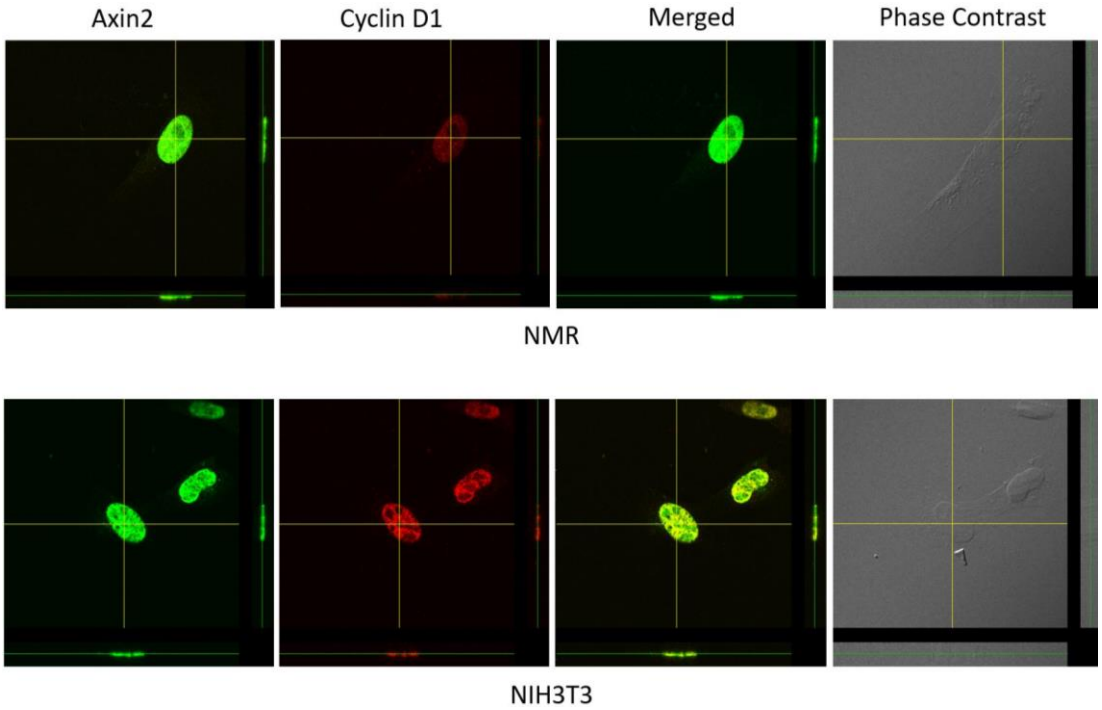

Supplementary Figure 4. Immunofluorescent results showing expression and localization of Axin2 in NSF and NIH3T3 cells.

ACKNOWLEDGEMENT

First and foremost, I am grateful to MEXT scholarship and Osaka University to prove financial support and offer me this opportunity to become a graduate student in Japan. I sincerely offer my gratitude to Osaka University for broadening both my horizons and global awareness.

I am indebted to my supervisor Professor Masato Okada for the knowledge and skills he has imparted, and his support and guidance for my project. Without his expertise, it would be more struggling to conduct and complete this project. I am also thankful to Sawada Miho and Akamatsu Kanko, Lab Technicians at RIMD, to provide the laboratory supplies required to run experiment in this project.

I want to thank my parents for encouraging me to pursue my dream and fulfil my aspiration. I am grateful to my mother for lifetime support and inspiration, and my father for instilling moral values and taught me to keep an open mind. Thank you so much for helping me achieve my goals.

Last but not least, I would like to acknowledge my lab partners, Yuriko Kurahashi and Kim Junhyeong, for helping and giving me advice throughout the lab session. Thank you very much.

By: Woei-Yaw Chee